A Review on Strategies Addressing Interface Incompatibilities in Inorganic All-Solid-State Lithium Batteries

Journal:	*Sustainable Energy & Fuels*
Manuscript ID	SE-REV-07-2019-000549.R1
Article Type:	Review Article
Date Submitted by the Author:	23-Aug-2019
Complete List of Authors:	Gurung, Ashim; South Dakota State University, Electrical Engineering and Computer Science Pokharel, Jyotshna; South Dakota State University, Department of Electrical Engineering and Computer Science Baniya, Abiral; South Dakota State University, Electrical Engineering and Computer Science Pathak, Rajesh; South Dakota State University, Electrical Engineering and Computer Science Chen, Ke; South Dakota State University, Electrical Engineering and Computer Science Lamsal, Buddhi; South Dakota State University, Electrical Engineering and Computer Science Ghimire, Nabin; South Dakota State University, Electrical Engineering and Computer Science Zhang, Wen-Hua; Institute of Chemical Materials, China Academy of Engineering Physics, ; Dalian Institute of Chemical Physics, Chinese Academy of Sciences, Zhou, Yue; South dakota state university, Electrical Enigneering Qiao, Qiquan; South Dakota State University, Center for Advanced Photovoltaics

A Review on Strategies Addressing Interface Incompatibilities in Inorganic All-Solid-State Lithium Batteries

Ashim Gurung,[1,†] Jyotshna Pokharel,[1,†] Abiral Baniya,[1,†] Rajesh Pathak,[1] Ke Chen,[1] Buddhi Sagar Lamsal,[1] Nabin Ghimire,[1] Wen-Hua Zhang,[2]* Yue Zhou,[1]* and Qiquan Qiao[1]*

[1]Department of Electrical Engineering and Computer Science, Center for Advanced Photovoltaics and Sustainable Energy, South Dakota State University, Brookings, SD 57007, USA
[2]Sichuan Research Center of New Materials, Institute of Chemical Materials, China Academy of Engineering Physics, Chengdu, P. R. China
*email: whzhang@caep.cn, yue.zhou@sdstate.edu, qiquan.qiao@sdstate.edu

†These authors equally contributed to this work.

Abstract
High flammability, susceptibility to unstable interfacial reactions and lithium dendrites growth make the currently employed liquid electrolyte systems in lithium batteries prone to severe safety concerns. Replacing the liquid electrolytes by solid-state versions is believed to be the ultimate solution to address the safety issues. Much research efforts have been dedicated to find solid-state electrolytes with excellent ionic conductivity comparable to the liquid counterparts and tremendous success has been achieved, especially with ceramic sulfide-based and oxide-based solid-state electrolytes. However, the other major constraint inhibiting the practical development of such solid-state batteries is the solid-solid interfaces. This review summarizes the notable approaches that have been implemented to address the interface incompatibilities of ceramic solid-state electrolytes with the battery electrodes. The focus will be on interfaces of sulfide and oxide solid electrolytes with both cathodes and metallic lithium anodes.

Keywords: Solid-state batteries, lithium batteries, interface, LGPS, LLZO, lithium dendrites, safety, lithium metal

1.   Introduction

Batteries have been a reliable conventional means of energy for portable devices. The advancement in smart electronics demands higher energy density of batteries. On the other hand, progress in acquirement of renewables for sustainable energy has also increased the demand in use of batteries to a great extent. Renewables such as solar and wind are intermittent in nature and require some sort of energy storage to address the issue. Batteries are considered to be the solutions for majority of the associated issues with high penetration of renewables into the electric grid[1]. Meanwhile, research in solar charging batteries has attracted much attention[2]. Furthermore, batteries have enabled electric vehicles as car manufacturers such as Tesla further advance their deployment. Each of this energy storage demanding applications has their own priorities for the properties of batteries required, as well as other figure of merits such as cost and safety. In particular, lithium-ion (Li-ion) battery chemistry has been a revolution since its commercialization by Sony Corporation in 1991, and still dominates the today's consumer electronics[3-5]. Extensive research has been conducted on further development of Li-ion batteries.[6-17] The commercial Li-ion battery chemistry composed of graphite anode/$LiNi_xCo_yMn_zO_2$(NMC) cathode can produce an energy density of 200-250 Wh/kg. However, it is imperative to investigate battery chemistries that can provide much higher energy density to meet the ever-growing energy demand[18].

One of the factors contributing to the lower energy density of the current Li-ion chemistry is the lower specific capacity of the graphite anode. Graphite has a theoretical specific capacity of 372 $mAhg^{-1}$. This has motivated to studies investigating higher capacity anode materials. Graphite facilitates lithiation based on intercalation mechanism, which accommodates one lithium ion per six carbon atoms. Materials that exhibit alloy-based lithiation have been heavily pursued[19-21]. Silicon is one such material and has a theoretical specific capacity of 4200 $mAhg^{-1}$ which is more than 10 times that of graphite[22]. However, silicon undergoes huge volume change ~400% during lithiation and mechanical breakage during delithiation. Several breakthrough strategies have been introduced such as use of silicon nanostructures, carbon coating, hollow protective cells and porous silicon[19, 23-27]. However, scaling up these nanostructures to a cost-effective production volume is a limitation.

Lithium metal is the ideal anode for Li-ion technology as it possesses the lowest negative electrochemical potential of -3.040 V vs standard hydrogen electrode and theoretical specific capacity of 3860 $mAhg^{-1}$.[4, 28, 29] Lithium metal was introduced as potential anode before the lithium-ion technology. However, the violent reactive and unstable nature of the lithium metal towards the organic electrolytes led to safety issues and eventually the Li-ion battery with graphite anode was introduced as a much safer alternative. Considering advances in nanotechnology, research on safe implementation of the lithium metal has been revived[17]. Research is focused on use of innovative approaches to restrain lithium dendrite growth and unstable solid electrolyte interphase layer associated with lithium metal as anode. Several attempts have been made, such as use of electrolyte additives, protective layer on top of lithium metal, porous current collector and use of lithium hosts[17, 30-34]. These research efforts are promising and should be encouraged at a much greater extent.

The other problem with the existing Li-ion technology is the low capacity of the cathodes. The conventional lithium metal oxides offer specific capacities of ~160-200 mAhg^{-1}. Therefore, when coupled with advanced anodes (Li), discrepancy exists in the potential capacities that can be delivered. This has led to research on potential high capacity cathodes such as sulfur and oxygen, namely Li-S and Li-O$_2$ batteries respectively[35]. These potential cathodes when paired against Li metal have high theoretical energy densities of 2500 Whkg^{-1} and 3500 Whkg^{-1} respectively[36, 37]. These advanced chemistries are also considered promising to achieve a low-cost storage system. However, several challenges exist in Li-S chemistry such as shuttle effect with dissolution of polysulfides, low electronic and ionic conductivity, volume change etc., while several promising efforts have been demonstrated addressing them[36, 38]. On the other hand, Li-O$_2$ is a much more complicated chemistry and still at infancy[37, 39, 40].

All these chemistries pursued for higher energy density have a common obstacle for their safe commercial deployment, which is associated to the use of liquid electrolytes. Solvents incorporated in these electrolytes are flammable and raise the safety concern for their use. In addition, the use of lithium metal in such liquid electrolyte environment poses significant risks of thermal runaway and thus safety[41, 42]. Besides, the liquid electrolytes tend to undergo uncontrollable side reactions with electrodes forming unstable interface that leads to severe capacity fading and low battery cycle life. All the aforementioned issues can be significantly suppressed with use of electrolytes in solid-state form which are non-flammable[43, 44]. Further, the use of solid-state electrolytes can provide stackable and high volumetric energy density. Some solid-state electrolytes also have very wide electrochemical stability window and can enable use of high voltage cathode materials to achieve higher energy density batteries[45]. In addition, solid-state electrolytes have also been proposed to suppress the growth of unwanted lithium dendrites when lithium metal anode is employed. The employment of solid-state electrolyte in a lithium metal battery is the ultimate goal to achieve a safe and high energy density storage system.

2.   Inorganic Electrolytes – Sulfides vs Oxides

The electrolyte in a Li-ion battery should have the characteristics such as (1) electronically insulating but ionically conducting, (2) undergo repeated cycling without chemical transformation i.e. exhibit good chemical/electrochemical stability, (3) good thermal stability over a wide range of operating temperature, (4) wide electrochemical operating window to enable high energy density, (5) good compatibility with electrodes and separator to accomplish efficient ion transport, (6) good mechanical stability to prevent or suppress lithium dendrites growth[46]. It is rather challenging to find an electrolyte system that satisfies all these requirements, however numerous efforts have been carried out in pursuit of such an electrolyte. Solid-state electrolytes can be categorized into two major groups namely, (i) polymers and (ii) inorganics (sulfides and oxides).

Polymers, with better flexibility can facilitate better interface formation with electrodes, but have low ionic conductivity at room temperature, limited thermal stability and narrow electrochemical window[46, 47]. In addition, solid polymer electrolytes can be more cost-effective

compared to the inorganics. From ionic conductivity prospect, inorganics especially the sulfides and oxides are promising candidates (as shown in Fig. 1 [43]) for further advancement of all-solid-state batteries, hence have attracted much attention.

Radar plots shown in Fig. 2a,b compare the sulfides and oxides with respect to various performance parameters for a solid-state electrolyte respectively. Solid sulfide electrolytes are capable of faster ionic conduction compared to oxide counterparts, owing to the presence of wider channels for ionic conduction in their structure. In addition, the lithium ions are more mobile in sulfides, attributed to the weaker affinity of lithium ions to sulfides[48]. As a result, the sulfides electrolytes have demonstrated the highest ionic conductivity among the solid electrolytes. The sulfides such as $Li_{10}GeP_2S_{12}$ (Fig. 2c) has already attained ionic conductivity of 12 $mScm^{-1}$ which is comparable to that of organic liquid electrolyte with ~10^{-2} Scm^{-1}.[49] Further, efforts have been carried out to substitute expensive Ge and as a result, another lithium superionic conductor $Li_{9.54}Si_{1.74}P_{1.44}S_{11.7}Cl_{0.3}$ has been reported with high ionic conductivity of 25 $mScm^{-1}$ [(50)]. Further, sulfides have better processing ability as they are comparatively easily deformable and have lower melting point. This enables densification of cold pressed sulfide pellets to form the required intimate particle-particle contacts, while very high temperature is required for their oxide counterparts. This also makes sulfides attractive from processing cost perspective.
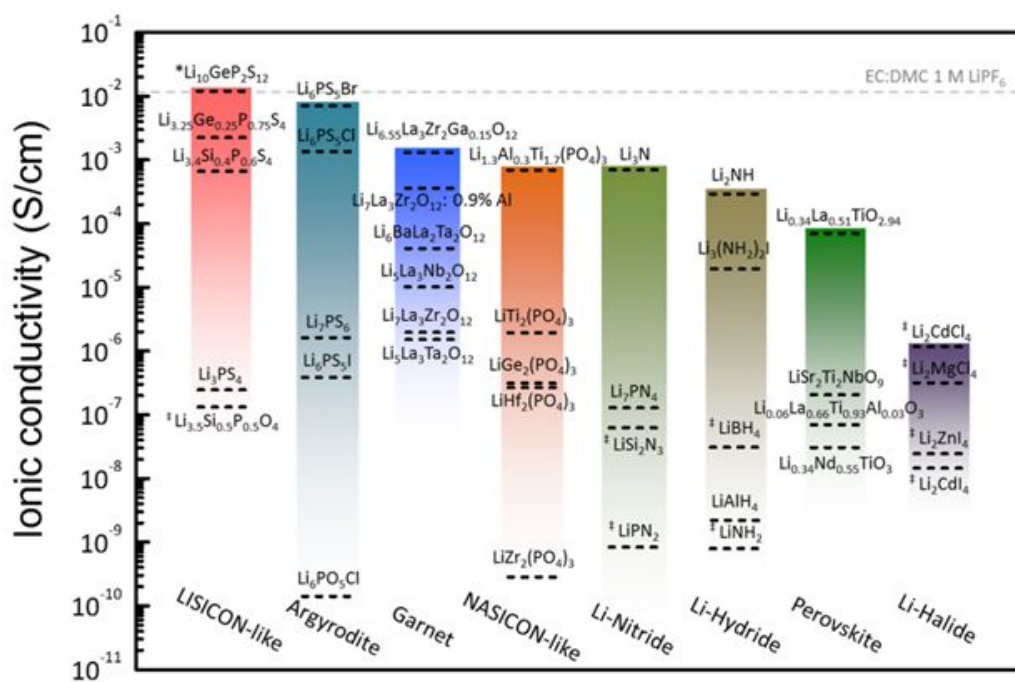
Fig. 1 Comparison of ionic conductivity of various solid-state lithium-ion conducting electrolyte families. Reproduced with permission from Ref.[43]. Copyright (2016) American Chemical Society.
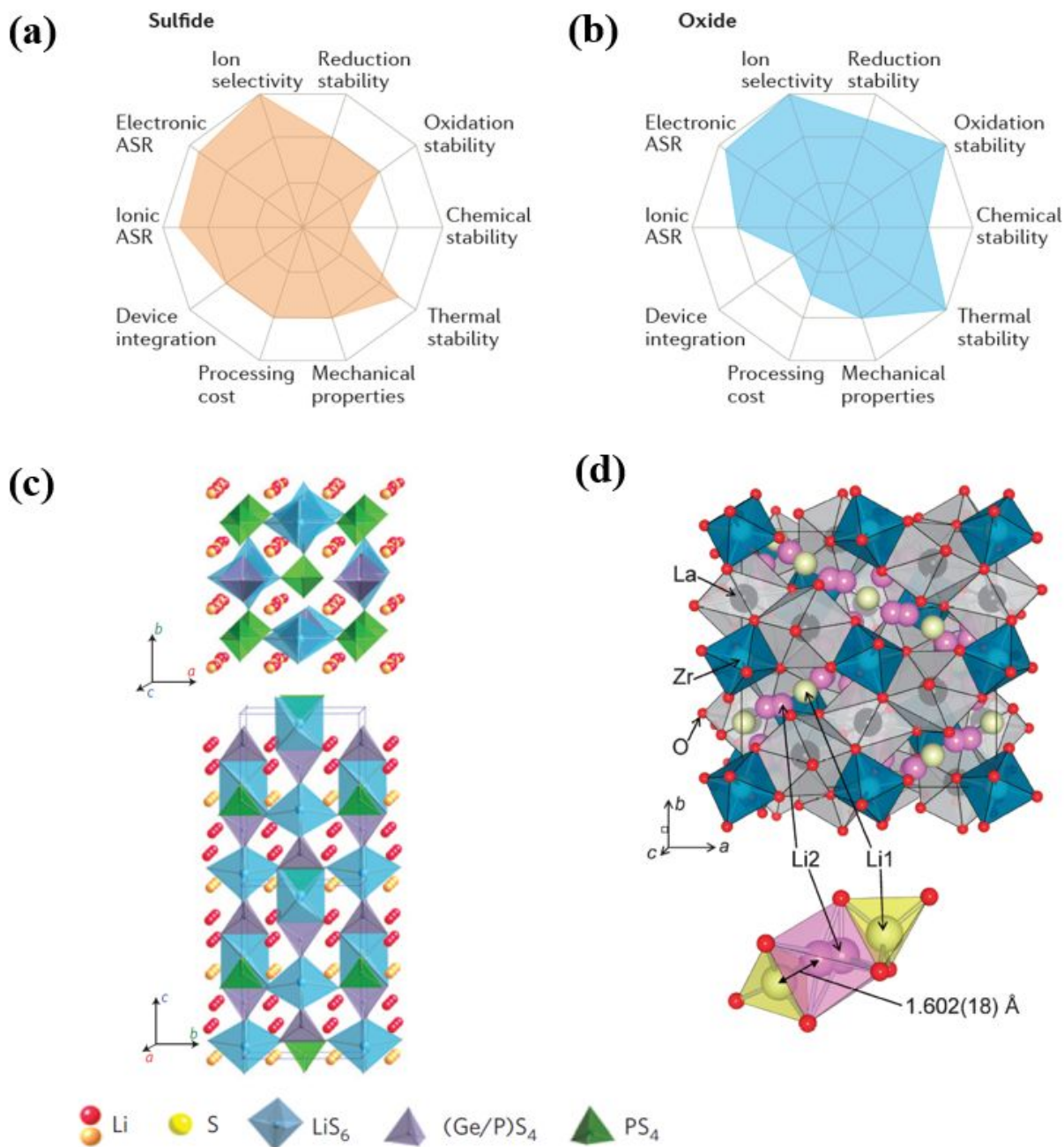
Fig. 2 Sulfides and oxides solid-state lithium ion conductors. Radar plots showing performance properties of (a) sulfide and (b) oxide. Reproduced with permission from Ref [44]. Copyright (2016) Springer Nature. Crystal structures of (c) $Li_{10}GeP_2S_{12}$ (Reproduced with permission from Ref [49]. Copyright (2011) Springer Nature) and (d) $Li_7La_3Zr_2O_{12}$ (Reproduced with permission from Ref [51]. Copyright (2011) Chemical Society of Japan.

However, the sulfides also have their own challenges. Most sulfide electrolytes are chemically prone to instability with water molecules generating toxic H_2S gas and therefore require an inert processing environment[52]. Further, sulfides are comparatively unstable towards lithium metal than oxides.

5

In comparison to the sulfide counterparts, solid oxide electrolytes demonstrate excellent chemical and thermal stability. The garnet type oxides such as $Li_7La_3Zr_2O_{12}$ (LLZO) show good stability against Li. Garnet type solid ionic conductors were first introduced by Thangadurai et al.[53] and later, garnet LLZO (Fig. 2d) was introduced with fast lithium ion conduction with ionic conductivity $(0.1 - 1 \text{ mScm}^{-1})$[54, 55]. Further, these garnet oxides are found to be stable against lithium metal and excellent thermal stability up to 900 °C[43]. However, these oxides have poor mechanical flexibility and high grain-boundary resistance. In addition, the processing of these electrolytes is expensive for large-scale production.

3.   Solid/Solid Interfaces

Liquid electrolytes can provide proper wettability to both anode and cathode in Li-ion battery. This facilitates efficient Li^+ transfer reactions into the bulk of the anode and cathode. Despite the high ionic conductivity of solid electrolytes such as the aforementioned sulfides, realization of an all-solid-state battery using such electrolytes is challenging as these solid electrolytes cannot effectively wet the battery electrode surface. This results in a high electrochemical impedance at electrode/electrolyte interface in case of the solid-state electrolytes. The chemical stability of the electrolyte plays a crucial role in determining the interfacial stability with the electrodes especially interface with the lithium metal electrode. The chemical stability of an electrolyte depends on the energy alignment of the electrolyte's lowest unoccupied molecular orbital (LUMO) or conduction band (CB) and the highest occupied molecular orbital (HOMO) or valence band (VB) with the chemical potential of anode and cathode[3]. The interphase products due to the interfacial reaction plays an important part in the Li^+ diffusion from the bulk electrolyte[56]. Several characterization techniques have been employed to characterize these interphase products. *In situ* X-ray photoelectron spectroscopy (XPS) characterization has revealed the presence of Li_3P, Li_2S and Li-Ge alloy in a Li/LGPS interface[57] and presence of Ti^{3+}, Ti^{2+} and Ti metal in a Li/lithium lanthanum titanate (LLTO) interface[58]. These insights will be a key role in further engineering of interface properties of the solid-state electrolyte with the anode and cathode in order to improve the interface.

Herein, interfaces with cathode and lithium metal electrodes focused on the oxides and sulfides solid electrolytes have been classified as: (i) Cathode/Sulfide electrolyte interface, (ii) Cathode/Oxide electrolyte interface, (iii) Lithium/Sulfide electrolyte interface and (iv) Lithium/Oxide electrolyte interface.

3.1. Cathode/Sulfide Electrolyte Interface

The interface of battery cathode and solid-state sulfide electrolyte is susceptible to elemental cross-diffusion and undesirable side reactions[59]. This makes the interface unstable leading to a large interfacial resistance. Especially, a space charge layer can be formed at the interface between an oxide cathode and the sulfide electrolyte, which originates due to the large difference in Li chemical potential in oxide and sulfide. This can be attributed to the much stronger bonding of lithium ions with oxides than with sulfides. Haruyama et al. studied the energy of exchanging ions between a typical cathode lithium cobalt oxide- $LiCoO_2$ (LCO) and β-Li_3PS_4 (LPS) solid

6

electrolyte and suggested that the mixing of elements Co and P is energetically favorable to the unmixed states at the interface[60]. Several efforts have been carried out to address the interface issue of sulfide solid electrolytes with battery cathodes.
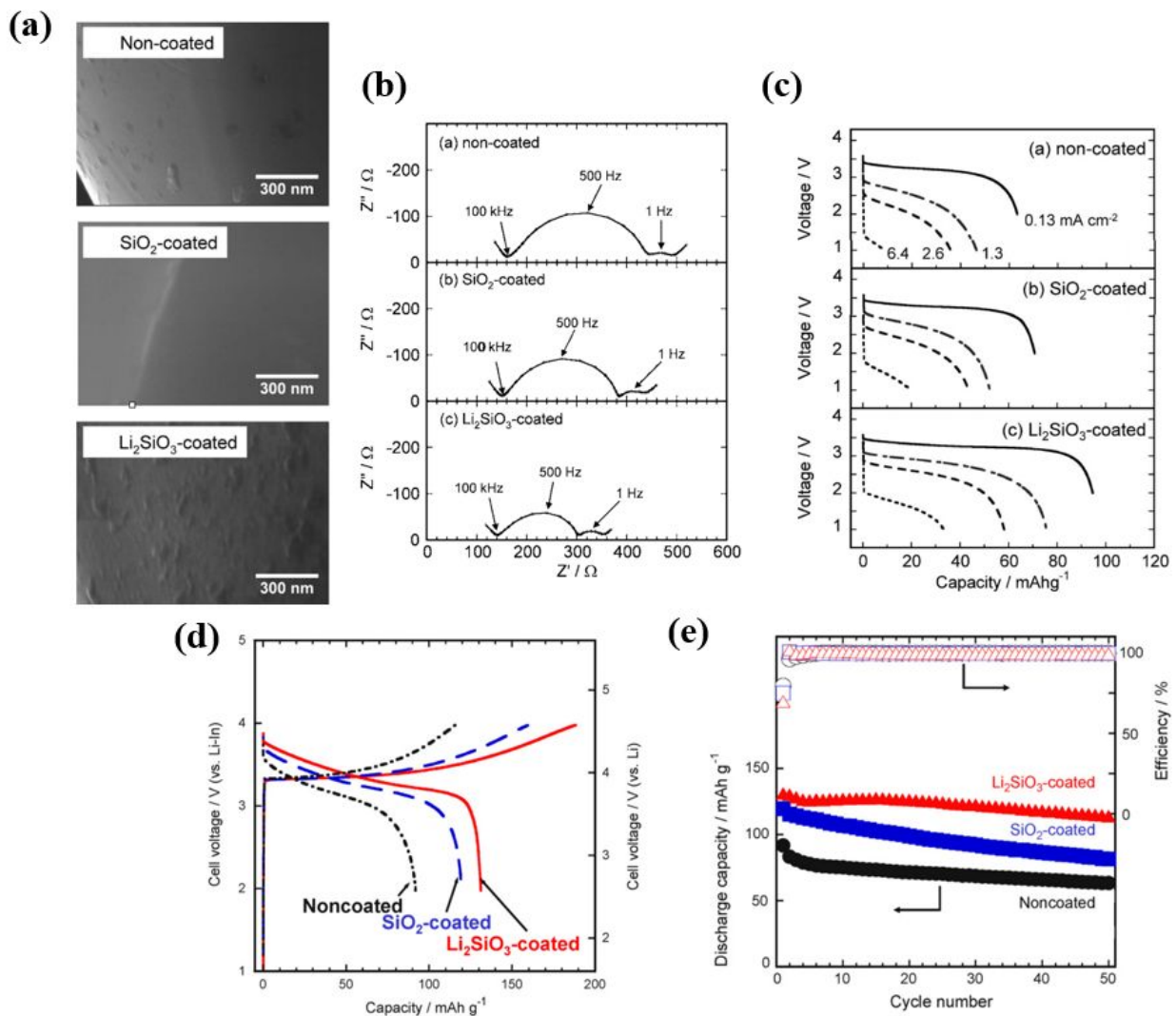
3.1.1.   Surface coating

Modification of the interface by applying a surface coating either on the sulfide electrolyte or the cathode particles has been extensively researched. These surface coatings can act as an effective buffer layer at the interface. Sasaki et al. developed a strategy to suppress the development of the space charge layer in the sulfide electrolyte by introducing an ionically conductive and electronically insulative thin film between the sulfide electrolyte and the oxide electrode[61]. The thin film was formed by spray coating of lithium titanate ($Li_4Ti_5O_{12}$ or LTO) on the surface of the LCO cathode particles. High rate performance of In-Li/LCO cells with LGPS sulfide electrolyte was observed for the coated samples, demonstrating 64% capacity retention at 5 mAcm^{-2} versus uncoated sample with only 4%. A graphite/LCO all solid-state cell with $70Li_2S-30P_2S_5$ sulfide electrolyte for the coated LCO cathode demonstrated comparable power densities with commercialized Li-ion batteries. Similar spray coated LTO on other oxide cathode $LiNi_{0.8}Co_{0.15}Al_{0.05}O_2$ (NCA) was investigated with $70Li_2S-30P_2S_5$ sulfide solid electrolyte[62]. However, the impact of the LTO coating on NCA was not as significant as on LCO. This was attributed to the much easier diffusion of Ni into LTO rather than Co. However, the LTO has a low ionic conductivity, thus its resistance significantly contributed to the electrode resistance, limiting the rate capability. With this into consideration, the same group also investigated other buffer layers such as $LiNbO_3$ and $LiTaO_3$ which has higher ionic conductivity in their amorphous state than LTO[63]. In addition, these coatings could be processed at preferred low temperature as high temperature treatment induces thermal diffusion of the elements. Theses coatings were also formed on LCO cathode particles by spray coating. The In-Li/LCO cell with $LiNbO_3$ coated LCO showed 74% capacity retention at 5 mAcm^{-2} versus uncoated sample with only 7%. Similar performance was observed in the case of the $LiTaO_3$ buffer layer. Similarly, the effect of $LiNbO_3$ coating on high voltage cathode $LiMn_2O_4$ was investigated[64]. It was concluded that a similar space charge layer exists between $LiMn_2O_4$ and sulfide electrolyte $Li_{3.25}Ge_{0.25}P_{0.75}S_4$ which limits the rate performance of all solid-state lithium batteries, and this can be suppressed by using coatings such as $LiNbO_3$.

Further, use of 2D nanosheets in the form of tantalum oxide (TaO_3) coated on the surface of a thin film LCO cathode formed by PLD was introduced[65]. TaO_3 nanosheet can function as an effective buffer layer as it can be very thin (~ 1 nm) and electronically insulative with a bandgap of 5.3 V. The TaO_3 nanosheets were deposited on the LCO surface by spin coating an acetonitrile suspension consisting of nanosheets in tetrabutylammonium hydroxide (TBAOH), followed by UV-light exposure for 12 h in N_2/O_2 environment to decompose the TBA ions. The TaO_3 as buffer layer decreased the resistance by two orders of magnitude in In-Li/LGPS/LCO system. The nanomesh structure of TaO_3 nanosheets can provide openings of 0.11 nm $\times$ 0.11 nm which enables lithium ion conduction through these channels. Sakuda et al. reported coatings of SiO_2 and Li_2SiO_3 on $LiCoO_2$ particles to improve the rate performance of all solid-state lithium

batteries (Fig. 3a)[66]. Sol-gel method was employed to obtain the coatings which consisted of mixing of respective Li_2SiO_3 sol and SiO_2 sol with LCO particles, followed by annealing at 350 °C for 30 min. In/$80Li_2S.20P_2S_5$/LCO cell was employed to evaluate the effectiveness of the coatings. The resistance contributed by the positive electrode side was decreased from 270 Ω for uncoated to 220 Ω for SiO_2 coating and 160 Ω for Li_2SiO_3 coating (Fig. 3b). The cell demonstrated a higher rate cycling performance for the coated LCO compared to the uncoated LCO (Fig. 3c). The lower interfacial impedance and higher rate performance of Li_2SiO_3 coated LCO versus SiO_2 coated LCO suggested that the ionic conductivity of the coating layer also contributes to achieve high-rate performance of all solid-state batteries. The effect of these coatings was further evaluated with cutoff voltage 4.6 V, where the coated LCOs demonstrated higher discharge voltages along with better cycling with higher charge/discharge capacities (Fig. 3d,e)[67].

Fig. 3 $LiCoO_2$ coating with sol-gel prepared SiO_2 and Li_2SiO_3 layers. (a) Scanning electron microscopy (SEM) images of surface of $LiCoO_2$ particles with and without the coatings; Performance of In/$80Li_2S.20P_2S_5$/$LiCoO_2$ solid-state cells with and without the coatings (b)

8

Nyquist plots and (c) Discharge voltage profiles at different current densities; Reproduced with permission from Ref [66] . Copyright (2008) The Electrochemical Society. (d) Charge-discharge voltage profiles and (e) Cycling capacities In/80Li$_2$S.20P$_2$S$_5$/LiCoO$_2$ solid-state cells with and without the coatings at higher cut-off voltage. Reproduced with permission from Ref [67]. Copyright (2009) Elsevier.

Further, sulfide coatings in the form of CoS and NiS on the LCO cathode particles were explored[68]. These sulfide coatings were formed by thermally decomposing their respective dithiocarbamato complexes on LCO particles at 400 °C for 2 h in N$_2$ atmosphere. All solid-state batteries utilized Li$_2$S-P$_2$S$_5$ sulfide electrolyte. These sulfide coatings mainly contributed to suppression of decomposition of the LCO electrode and Li$_2$S-P$_2$S$_5$ sulfide electrolyte, and formation of an interface with high electronic and lithium-ion conductivity. This resulted in significant decrease in interfacial resistance between LCO and the electrolyte. Further, the group prepared LiFePO$_4$ glass ceramic electrode with an amorphous surface layer consisting of Li, Fe, Nb, P, O, and C elements and 80Li$_2$S-20P$_2$S$_5$ sulfide-based electrolyte for an all solid-state battery[69]. The solid-state cell based on this modified LiFePO$_4$ delivered higher capacities compared to the commercial LiFePO$_4$. It was observed that the amorphous surface layer improved interfacial properties between LiFePO$_4$ electrode and Li$_2$S-P$_2$S$_5$ solid electrolyte. Machida et al. employed Li$_2$O-ZrO$_2$ coated LiNi$_{0.8}$Co$_{0.15}$Al$_{0.05}$O$_2$ (NCA) cathode to suppress the mutual diffusion at the cathode/electrolyte interface and reduce the interfacial resistance[70]. Full cells with graphite/Li$_2$S-P$_2$S$_5$ (80:20 mol%)/NCA were tested. The NCA cathode composite consisted of Li$_2$O-ZrO$_2$ coated NCA (59 wt%), Li$_2$S-P$_2$S$_5$ (80:20 mol%), conductive carbon based on carbon nanotube (5 wt%) and hydrocarbon polymer binder (2 wt%). The coated NCA cells showed decrease in interface resistance that contributed to improvement in the discharge rate performance compared to the uncoated NCA. Similarly, coating of higher capacity cathode oxide Li(Ni$_{1/3}$Mn$_{1/3}$Co$_{1/3}$)O$_2$ "NMC" has also been investigated. Inert metal oxides such as Al$_2$O$_3$ and ZrO$_2$ have been employed as coating on NMC cathode to improve the interfacial stability of the NMC cathode and sulfide solid electrolytes[71].

However, the poor ionic conductivity of these inert metal oxides restrains achievement of optimum rate capability performance of all-solid-state batteries. As a solution, use of LiAlO$_2$ coating on NMC has been suggested as LiAlO$_2$ with higher ionic conductivity can provide an effective Li$^+$ conduction pathway from NMC to solid electrolyte[72]. A sol-gel method was employed to coat the LiAlO$_2$ layer on the NMC cathode particles and the sol gel mixture was heated at various temperature range of 250-750 ºC for 1 h under O$_2$ environment to decompose the organic components. The performance of the coating on NMC was evaluated by using solid-state cells comprising of the coated NMC cathodes, amorphous Li$_3$PS$_4$ as solid electrolyte and Li$_{4.4}$Si as anodes. The 1 mol% LiAlO$_2$ coating heat treated at 350 ºC showed the minimum interfacial impedance. The cell with 1 mol% LiAlO$_2$ coated NMC exhibited superior cycling stability with 134 mAhg^{-1} (1st discharge) and 124 mAhg^{-1} (400th discharge) compared to uncoated NMC with 102 mAhg^{-1} (1st discharge) and 74 mAhg^{-1} (250th discharge), suggesting the suppression of unwanted reaction between Li$_3$PS$_4$ and NMC by the LiAlO$_2$ coating.

Further, Kim et al. presented an interesting observation with use of lithium carbonate (Li_2CO_3) as coating on LCO cathode powders[73]. Li_2CO_3, which is a spontaneous coating formed during synthesis of LCO is unfavorable in conventional liquid Li-ion batteries as it is electrochemically inactive. Therefore, post treatment of LCO is done to remove Li_2CO_3 from the surface of LCO powders. However, Li_2CO_3 is also a component of the solid electrolyte interphase (SEI) layer that prevents further electrolyte decomposition in the cell. Considering this, Li_2CO_3 coated LCO cathodes were investigated for all solid-state batteries employing Li_2S-P_2S_5 sulfide electrolyte. The Li_2CO_3 coating on LCO cathodes was prepared using mixtures of lithium hydroxide and LCO powder heated at low temperature of 400 ºC under CO_2 for 3h. The cell with 4 wt% Li_2CO_3 coated LCO exhibited a discharge capacity of 137 mAhg^{-1} at 0.05 C and 86.4 mAhg^{-1} at 0.5 C compared to uncoated LCO with 62.1 mAhg^{-1} at 0.05 C and 13.9 mAhg^{-1} at 0.5 C. These results suggest that an appropriate amount of Li_2CO_3 coating as a physical barrier can contribute to enhancement in cell reversibility and interfacial stability by decreasing the interfacial impedance during charge/discharge.

3.1.2. Interface softening

One of the major obstacles for the implementation of solid-state electrolyte is its wettability towards the battery electrodes resulting in small contact area between the active material and electrolyte. Kitaura et al. employed the softening of $80Li_2S.20P_2S_5$ glassy electrolyte to increase the active contact area between the active material and solid electrolyte[74]. The $80Li_2S.20P_2S_5$ glassy electrolyte was converted to a supercooled liquid state by hot pressing and this viscous liquid was used to form contact with the active materials LTO and LCO. It was observed that a reaction occurred between the viscous electrolyte and LCO, which was then overcome by a $LiNbO_3$ coating on LCO. A higher reversible capacity of 120 mAhg^{-1} was observed for an all-solid-state battery (LTO/$80Li_2S$-$20P_2S_5$ sulfide electrolyte/$LiNbO_3$ coated LCO) that employed hot pressing in comparison to cold pressing with only 50 mAhg^{-1}.

3.1.3. Electrolyte Infiltration

Sulfide electrolytes are reactive towards the common polar solvents used for the wet slurry process to fabricate electrodes for lithium batteries. Therefore, to obtain a composite electrode for all solid-state batteries, Kim et al. demonstrated infiltration of solution processable sulfide electrolyte into the conventional electrodes of Li-ion batteries[75]. For this, the conventional LCO and graphite electrodes prepared by slurry casting were dipped into a Li_6PS_5Cl (LPSCl) sulfide electrolyte solution in ethanol, followed by drying in argon environment, vacuum annealing at 180 ºC and cold pressing under 770 MPa (Fig. 4a). The LPSCl infiltrated LCO (Fig. 4b) and graphite electrodes demonstrated high reversible capacity of 141 mAhg^{-1} and 364 mAhg^{-1} at 0.1 C and 30 ºC (Fig 4c,d). The electrochemical performance of the LPSCl electrodes were found to be superior to conventionally prepared (dry-mixed and slurry-mixed) electrodes for solid state batteries and comparable to that of liquid electrolyte cells. The superior performance was attributed to the formation of intimate ionic contacts formed by ionic percolation pathways.
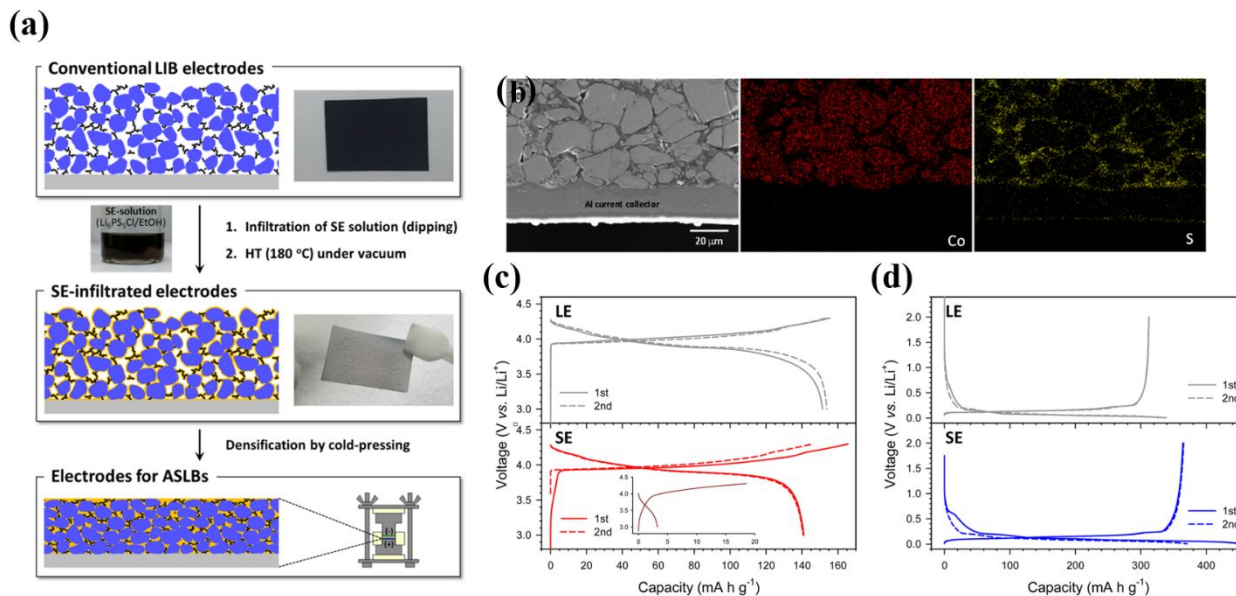
Fig. 4 Solution processible Li_6PS_5Cl sulfide electrolyte infiltrated into battery electrodes. (a) Schematic depicting the approach; (b) Cross-sectional SEM image of the infiltrated LCO battery electrode and elemental mapping of Co and S; Charge/discharge voltage curves of (c) LCO/Li-In and (d) Gr/Li-In half cells at 0.1 C with liquid (LE) and infiltrated solid-state (SE) electrolytes. (Inset shows voltage profiles for LCO without solid-state electrolyte infiltration). Reproduced with permission from Ref [75]. Copyright (2017) American Chemical Society.

3.1.4. Electrolyte coating on cathodes

The cathodes in all-solid-state batteries require a conductive pathway to the solid electrolyte. The conventional approach for cathodes in all solid-state batteries is to use a composite of solid electrolyte powder mixed with the cathode. The other promising and effective approach is the coating of the cathode powder with solid-state electrolyte. Sakuda et al. demonstrated $80Li_2S$-$20P_2S_5$ sulfide electrolyte (1 wt%) coating on $LiNbO_3$ coated LCO powder by PLD (Fig. 5a,b)[76]. The electrolyte coated LCO cells were able to reversibly charge and discharge with a reversible capacity of 30 mAhg^{-1} for 100 cycles while the non-coated LCO cells were not. This performance was further improved by controlling the amount of coating and heat treatment of the $80Li_2S$-$20P_2S_5$ sulfide electrolyte coated LCO[77]. The amount of coating when increased from 40 min to 120 min improved the reversible capacity from 35 to 65 mAhg^{-1} and further heat treatment at 200 ºC improved to 69 mAhg^{-1}. The heat treatment led to increase in ionic conductivity of the coating. Meanwhile, all-solid-state cells using a mixture of the sulfide electrolyte (20 min) coated LCO with sulfide electrolyte particles (90/10 wt%) delivered a much lower interfacial resistance and reversible capacity of 95 mAhg^{-1} which was also superior to cells with uncoated (20 mAhg^{-1}) and $LiNbO_3$-coated LCO (60 mAhg^{-1}) mixed with sulfide electrolyte particles (Fig. 5c). This approach demonstrated effective formation of lithium-ion conducting pathway in the cathode composite for all solid-state batteries. In addition, this approach of sulfide coating on cathodes facilitates use of significantly less amount of sulfide electrolyte to form the cathode composite in comparison to the traditional approach of mixing sulfide electrolyte powder with cathode

powder to form the composite. This decrease in the amount of the sulfide electrolyte can contribute to increase in energy density of the all-solid-state batteries.
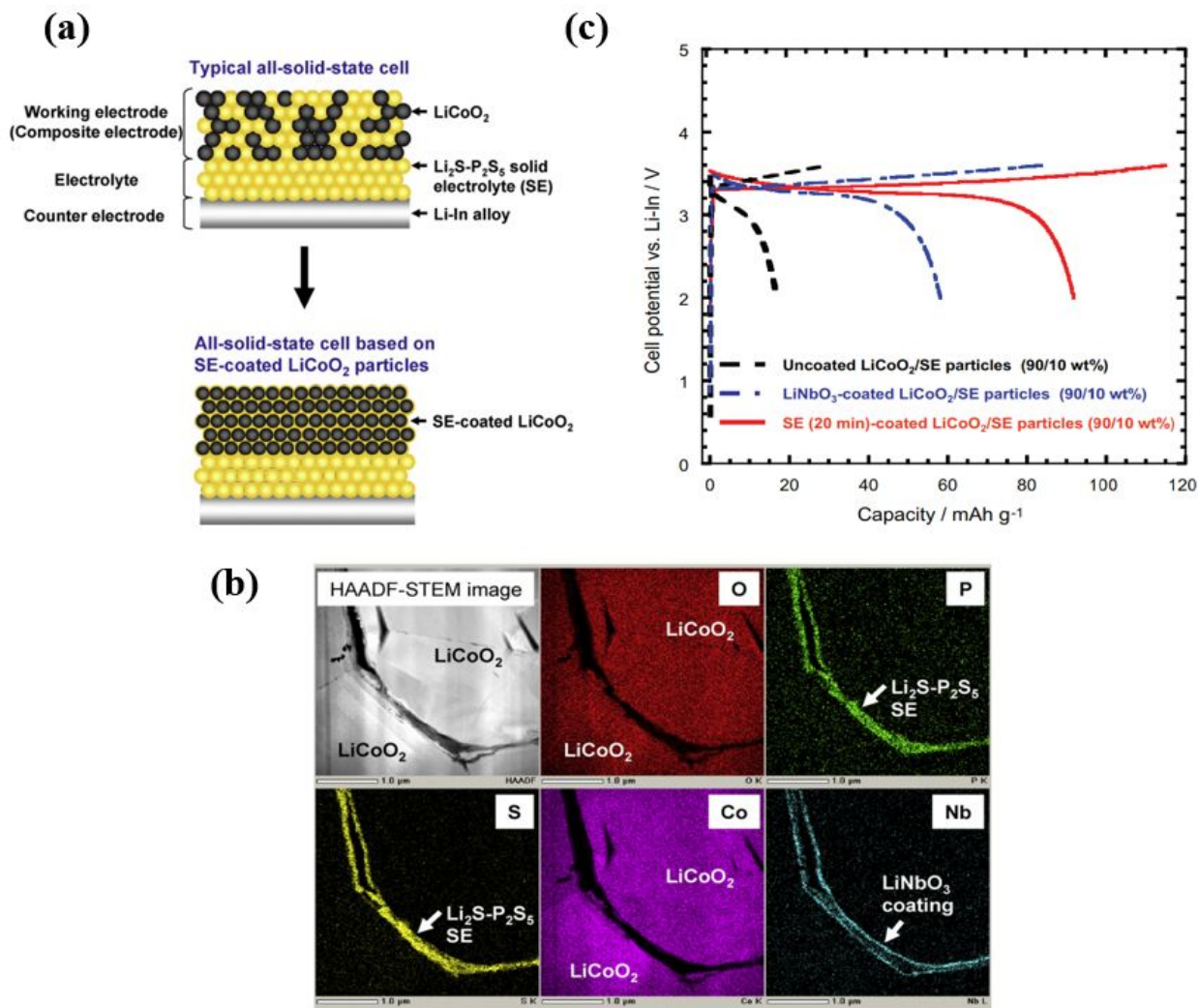
Fig. 5 $LiCoO_2$ particles coated with pulsed layer deposited $Li_2S-P_2S_5$ solid electrolyte. (a) Schematic showing the approach; (b) Elemental mapping of the solid electrolyte coated $LiCoO_2$ after 450 cycles; (c) Charge-discharge voltage profiles of all-solid-state cells In/solid-state electrolyte/$LiCoO_2$ consisting of 90 wt% $LiCoO_2$ and 10 wt% solid electrolyte particles using uncoated $LiCoO_2$, $LiNbO_3$-coated $LiCoO_2$ and solid-electrolyte (20 min) coated $LiCoO_2$. Reproduced with permission from Ref [77]. Copyright (2011) Elsevier.

To further enhance the performance of the all-solid-state batteries, thin film coatings of sulfide electrolyte such as $Li_4GeS_4-Li_3PS_4$ that possess even higher ionic conductivity $> 10^{-3}$ Scm^{-1} at 25 ºC were considered[78]. Similar PLD method was employed to deposit the sulfide electrolyte on $LiNbO_3$ coated LCO cathodes. Heat treatment of the sulfide coated LCOs led to enhancement in ionic conductivity as well as decrease in number of voids in the composite cathode electrode. This observation was complemented by (i) decrease in the interfacial resistance between the sulfide electrolyte coating layer and positive electrode, (ii) increase in

reversible capacity of In/80Li$_2$S-20P$_2$S$_5$/LCO from 67 to 82 mAhg^{-1} and (iii) enhancement in the rate capability of the cells.

Further, Aso et al. explored the deposition of Li$_2$S$_5$ -P$_2$S$_5$ sulfide electrolyte coating on NiS grown on vapor grown carbon nanofiber (VGCF) by PLD as a composite electrode for all-solid-state battery[79]. The VGCF facilitates continuous electronic conduction pathways in the composite electrode. The PLD deposited coating of 80Li$_2$S-20P$_2$S$_5$ on the NiS-VGCF composite provides lithium ion conduction pathways for the NiS active material. The solid-state cell based on solid electrolyte coated NiS-VGCF composite/80Li$_2$S-20P$_2$S$_5$/Li-In delivered high 2nd cycle discharge capacity of 240 mAhg^{-1} at 1 C rate versus cell compared to the uncoated NiS-VGCF with only 100 mAhg^{-1}. This suggested the favorable electron and lithium ion conduction paths achieved by the sulfide electrolyte coated NiS-VGCF. Similarly, Xu et al. prepared MoS$_2$/Li$_7$P$_3$S$_{11}$ composite cathode by coating Li$_7$P$_3$S$_{11}$ solid electrolyte layer on MoS$_2$ particles using solution processing method[80]. The MoS$_2$/Li$_7$P$_3$S$_{11}$ electrode exhibited an initial discharge capacity of 868.4 mAhg^{-1} and reversible charge capacity of 669.2 mAhg^{-1} with Coulombic efficiency of 77.1% versus the untreated MoS$_2$ electrode with initial discharge capacity of 740 mAhg^{-1} followed by rapid capacity fade during cycling.

3.1.5. Sulfur-based nanocomposite positive electrode

A rather compatible cathode for a sulfide solid electrolyte would be the sulfur-based cathode as active material compared to the oxide cathodes. Hayashi et al. reported an approach to form nanocomposites of NiS active material with solid sulfide electrolyte 80Li$_2$S-20P$_2$S$_5$ that accomplishes an intimate contact area between solid electrolyte and positive electrode for all-solid-state batteries[81]. Nanosized NiS embedded into the 80Li$_2$S-20P$_2$S$_5$ sulfide electrolyte was obtained by mechanochemical method. This approach of preparing the composite electrode delivered higher charge/discharge capacity compared to the cell with electrode formed by conventional mixing of electrode and electrolyte powders. Similarly, Li$_7$P$_3$S$_{11}$ electrolyte particles anchored on cobalt sulfide nanosheets via an *in situ* liquid-phase approach was demonstrated by Yao et al. (Fig. 6a)[82]. The anchored nanosized Li$_7$P$_3$S$_{11}$ electrolyte particles (with reduced particle size ~ 10 nm) onto the surface of cobalt sulfide nanosheets increased the contact area between the electrolyte and active materials, enabling reduction of interfacial resistance (Fig. 6c). The enhancement in interface led to an all-solid-state cell (Fig. 6b) exhibiting high rate capability (Fig. 6d,e) with 421 mAhg^{-1} at 1.27 mA cm^{-2} after 1000 cycles (Fig. 6f) and high energy and power densities of 360 Whkg^{-1} and 3823 Wkg^{-1} at current densities of 0.13 and 12.73 mA cm^{-2}, respectively versus pristine cobalt sulfide cathode.
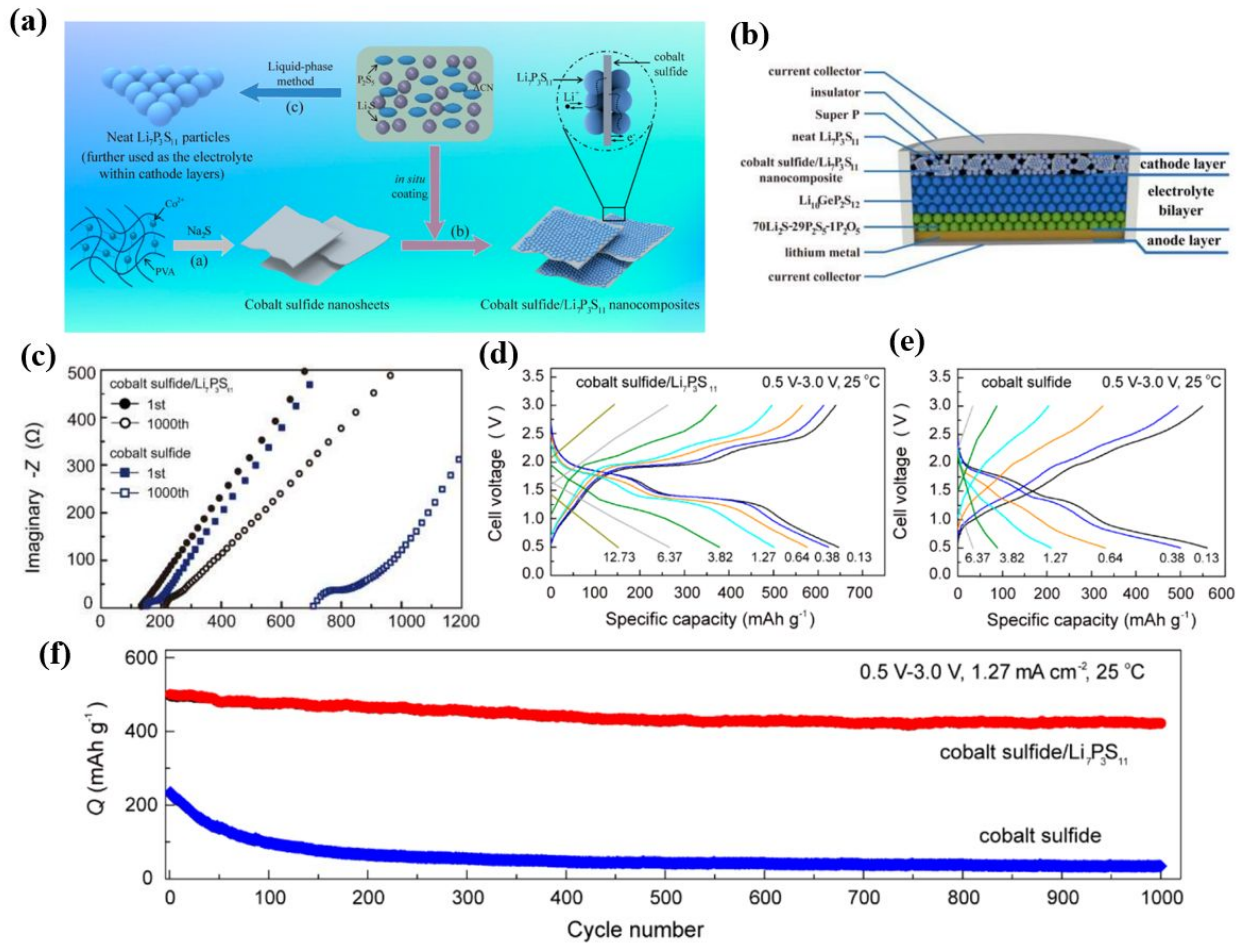
Fig. 6 Cobalt sulfide-$Li_7P_3S_{11}$ nanocomposites as positive electrode. (a) schematic showing the synthesis process; (b) schematic showing the all-solid-state Li-ion battery under study; (c) Nyquist plots showing comparison of Cobalt sulfide-$Li_7P_3S_{11}$ nanocomposites with cobalt sulfide at 1st and 1000th cycles at current density of 1.27 mAcm^{-2}; Charge/discharge voltage profiles of the solid-state cells at various rates in voltage range of 0.5-3.0 V at 25 °C with (d) Cobalt sulfide-$Li_7P_3S_{11}$ nanocomposites and (e) cobalt sulfide nanosheets; (f) Cycling performance of the cells. Reproduced with permission from Ref [82]. Copyright (2016) American Chemical Society.

The fact that Li-S battery technology employs sulfur which is also a constituent in sulfide electrolytes makes it appealing to explore sulfur positive electrode. Nagao et al. investigated the use of sulfur-carbon composite with Li_2S-P_2S_5 sulfide electrolyte for all-solid-state Li-S batteries[83]. The composite of sulfur-carbon with Li_2S-P_2S_5 was obtained by mechanical milling of sulfur (S), acetylene black (AB) and Li_2S-P_2S_5 solid electrolyte (SE), which facilitated amorphization of sulfur reduction of the electrode particle size. The all-solid-state Li-S cells of Li-In/80Li_2S-20P_2S_5 glass-ceramic/S with three different composite S electrode were studied and compared namely, i) S+AB+SE (obtained by grinding all three in a mortar), ii) S-AB+SE (obtained by milling S and AB, followed by grinding S-AB composite and SE in mortar) and iii) S-AB-SE (obtained by milling the mixture of S-AB composite and SE). The cell with S-AB-SE

14

electrode showed significant improvement in reversible capacity with charge/discharge capacity of 1550/1220 mAhg^{-1} (1st cycle) compared to S+AB+SE (<100 mAhg^{-1}) and S-AB+SE (< 300 mAhg^{-1}). In addition, the cycling capacity of the cell with S-AB-SE electrode was excellent exhibiting reversible capacity of 853 mAhg^{-1} at 1.3 mAcm^{-2} and 996 mAhg^{-1} at 0.64 mAcm^{-2} for 200th cycle. The superior performance was attributed to the intimate electronic contact and ionic contact formed among the three components, S, AB and SE achieved by the mechanical milling approach. The same group investigated the Li$_2$S active material for all-solid-state Li-S battery using similar approach of mechanical milling to obtain Li$_2$S composite electrode[84]. The all-solid-state In/80Li$_2$S-20P$_2$S$_5$ glass-ceramic/Li$_2$S with three different composite Li$_2$S electrode were studied and compared namely, i) Li$_2$S+AB+SE (obtained by grinding all three in a mortar, ii) Li$_2$S-AB+SE (obtained by milling S and AB, followed by grinding S-AB composite and SE in mortar and iii) Li$_2$S-AB-SE (obtained by milling the mixture of S-AB composite and SE). The cell with Li$_2$S-AB-SE electrode exhibited reversible capacity of 700 mAhg^{-1} for 10 cycles compared to Li$_2$S+AB+SE (< 10 mAhg^{-1}) and Li$_2$S-AB+SE (only 170 mAhg^{-1}). Further, the effect of particle size of Li$_2$S active material was studied using non-milled (particle size >100 μm) and milled (particle size < 1 μm) Li$_2$S particles. The Li$_2$S-AB-SE electrode with milled Li$_2$S delivered higher reversible capacity of 795 mAhg^{-1} and a superior rate performance compared to the non-milled Li$_2$S. The reduction of the particle size of Li$_2$S and intimate contact between the three components Li$_2$S, AB and SE contributed to the excellent performance of the all solid-state Li-S battery. Further, the microstructural changes of the Li$_2$S-AB-SE composite electrode upon cycling was studied[85]. It was concluded that the Li$_2$S active particles less than 10 nm were able to reversibly change from crystalline to amorphous upon lithiation and amorphous to crystalline upon delithiation, suggesting the reversible reaction of $Li_2S \leftrightarrow S + 2Li^+ + 2e^-$ taking place. It is significantly important to have the Li$_2$S active particles less than 10 nm be well-dispersed in the composite electrode consisting of AB and SE particles.

Han et al. introduced the concept of using a single material for all-solid-state batteries where they demonstrated use of LGPS as both anode and cathode after mixing with carbon additives (Fig. 7a,b)[86]. The Li-S and Ge-S components in LGPS can act as cathode and anode of the battery respectively. The area-specific interfacial resistance for the single-LGPS battery was comparable to that of the liquid electrolyte battery, despite the higher loading and larger thickness of the active material. High reversible capacities of 275 mAhg^{-1} and 253 mAhg^{-1} were observed for the LGPS as cathode and anode respectively with excellent rate capability performance (Fig. 7c-f). The single LGPS battery was able to exhibit a reversible capacity of 104 mAhg^{-1} (Fig. 7g). Similar concept can be explored for other solid electrolyte systems as well.
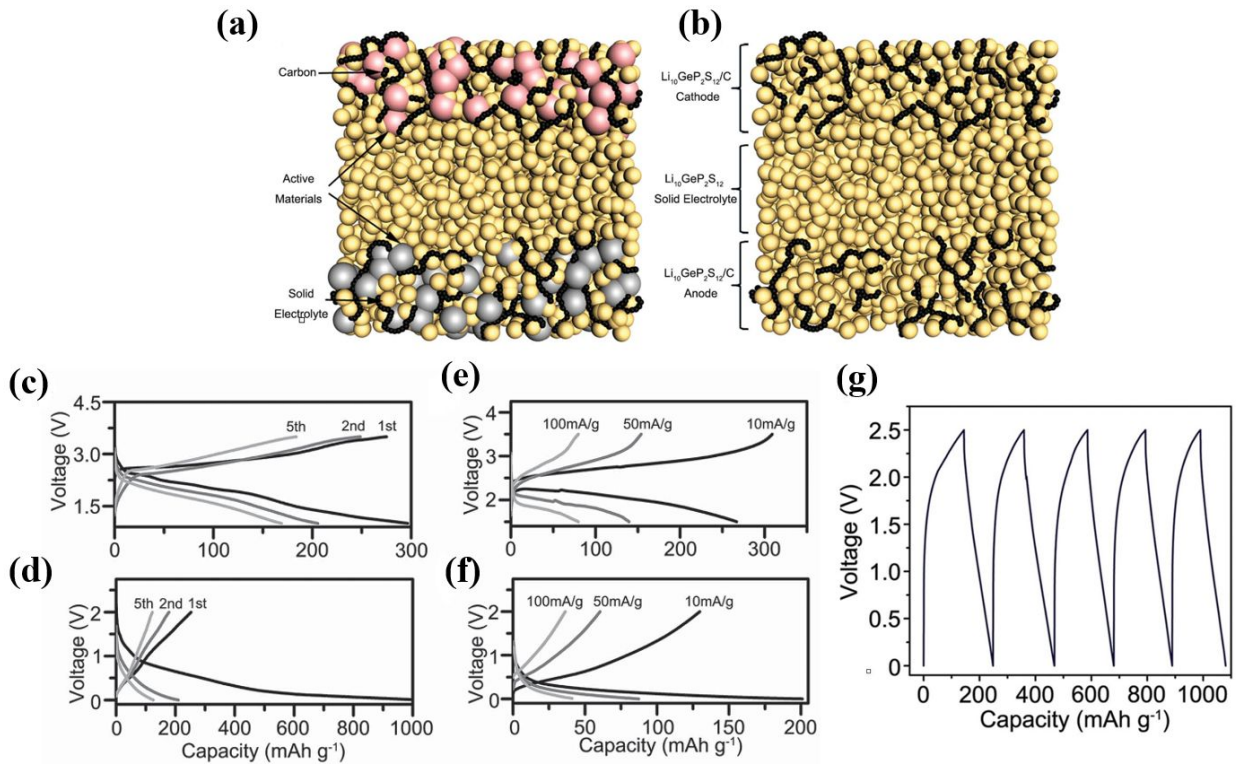
Fig. 7 Single material for all solid-state battery. Schematic showing comparison between (a) typical and (b) single-material ($Li_{10}GeP_2S_{12}$) all-solid-state battery; Charge/discharge voltage profiles of Li/LGPS/LGPS-C solid-state cells in voltage range of (c) 1.5-3.5 V for cathode and (d) 0.0-2.0 V for anode at current density of 10 mAg^{-1}; (e, f) Charge/discharge voltage profiles of Li/LGPS/LGPS-C solid-state cells at different current densities; (g) Charge/discharge voltage profiles of the single-LGPS battery at current density of 10 mAg^{-1} in voltage range of 0.0-2.5 V. Reproduced with permission from Ref [86]. Copyright (2015) John Wiley and Sons.

3.2. Cathode/Oxide electrolyte Interface

The high interfacial resistance at the cathode/electrolyte interface can be due to (1) poor contact between (a) active cathode material and solid electrolyte in the bulk of the cathode composite and (b) cathode layer and electrolyte layer, (2) electrochemical cycling instability between the cathode active material and solid electrolyte, and (3) volume change of the electrode materials causing interfacial stress/strain. This cathode/electrolyte interfacial problem is even more severe in the case of the ceramic oxides compared to their sulfide counterparts. The objective would be to obtain an excellent fine physical contact between the cathode and electrolyte. Numerous efforts have been reported on modification of this interface.

3.2.1. Vacuum deposition of a thin film cathode on oxides

One of the attempts to realize a good interfacial contact between solid oxide electrolytes with cathode has been the use of vacuum deposition of a thin-film cathode on the solid oxide electrolytes. Toyota R&D Labs Inc demonstrated use of pulsed laser deposited LCO cathode thin film (~ 500 nm) on top of $Li_{6.75}La_3Zr_{1.75}Nb_{0.25}O_{12}$ (LLZONb)[87]. The cathode thin film deposition

approach demonstrated low interfacial resistance of 170 Ωcm^{-2} for LCO/LLZONb/Li cell that is comparable to that of Li-ion batteries with liquid electrolyte. The cell exhibited a charge/discharge capacity of 130/129 mAhg^{-1}, accounting to 90% of the theoretical capacity of LCO. Likewise, Matsuyama et.al reported a thin film electrode of amorphous TiS$_4$ (α. TiS$_4$) (~400nm) by pulse laser deposition on garnet type solid electrolyte[88]. The dense α. TiS$_4$ electrode showed good contact between the electrode and the electrolyte with the conductivity of 1.0x 10^{-4} Scm^{-1} at 25 °C. All solid-state cell of Li/LLZ/α. TiS$_4$ at 25 °C showed reversible capacity of about 500 mAhg^{-1} of α. TiS4 at 0.010 mA cm^{-2} and good cycling performance for 15 cycles. A thin film of LCO was sputtered onto Li$_2$O$-$Al$_2$O$_3$$-SiO_2$$-P_2O_5$$-TiO_2$$-GeO_2$ (LICGC) NASICON-type glass ceramic solid electrolyte substrate and was annealed to observe the microstructural change in LCO cathode and LCO/electrolyte interface[89]. Solid-state cell with LCO/NASICON electrolyte interface showed stable performance during cycling. However, capacity fading was observed due to the degradation of the NASICON-type electrolyte in contact with the lithium metal anode.

### 3.2.2. High temperature co-sintering of cathode with oxides

The limitation of vacuum deposition of cathodes on oxides is the lower thickness of the cathodes. To realize higher bulk energy density, a much thicker cathode (~ 100 microns) would be required. A thicker cathode can be easily accomplished using the traditional slurry-based coating method. However, this conventional approach does not facilitate a sufficient interfacial contact of the coated cathode and the solid oxide.

To address this, Goodenough et al. studied sintering of LCO on LLZO pellet at 700 °C and obtained a low capacity of only 35 mAhg$^{-1(90)}$, while the theoretical capacity of LCO is ~ 140 mAhg^{-1}. However, chemical instability between the cathode and LLZO is most likely to occur that again leads to a highly resistive interphase. This chemical instability was attributed to the elemental cross-diffusion and formation of a tetragonal LLZO phase at the interface. It is important to identify the reactions that take place between oxide cathode and oxide electrolytes, and their decomposition products in these high temperature cosintering approach to form dense cathodes. This can help for better interfacial design of a solid-state battery. Taking this into consideration, Miara et al. studied decomposition reactions that take place when cosintering high voltage spinel cathode materials Li$_2$NiMn$_3$O$_4$ and Li$_2$FeMn$_3$O$_8$ and LiCoMnO$_4$ with Li$_{6.6}$La$_3$Zr$_{1.6}$Ta$_{0.4}$O$_{12}$ (LLZTO).[91] Thermal analysis techniques and X-ray diffraction along with ab initio calculations were employed for the study. It was found that the LLZTO was not compatible with spinel cathodes even at 600°C. The lithium and oxygen of the LLZTO were responsible to react with the cathodes to form insulation phases in the form of La$_2$Zr$_2$O$_7$, La$_2$O$_3$, La$_3$TaO$_7$, TiO$_2$ and LaMnO$_3$ which contribute to increase the interfacial impedance. Liu et al. employed rapid thermal annealing technique of cathode on garnet by supplying voltage to a suspended rectangular piece of carbon paper (1 cm length, 0.8 cm width and 250 μm thickness) on glass substrate between two copper electrodes with conductive silver paste[92]. The garnet solid electrolyte was put on the glass substrate beneath the carbon paper during rapid thermal annealing, which decreased the interfacial charge transfer resistance from 2.5x10^4 Ωcm^2 to 71

Ωcm^2 at room temperature. Further, the interfacial resistance decreased by 5.5 times from 170 to 31 Ωcm^2 at 100 °C.

3.2.3. Use of solid electrolyte into the cathode layer

The high chemical instability of LCO/LLZO interface at high temperature has been addressed by use of ionic conductor into the cathode. Ohta et al. in 2013 introduced sintering additive Li_3BO_3 (LBO) that is chemically stable with LCO and LLZONb[93]. LBO is an ionic conductor with a low melting point (ca. 700 ºC). The LBO when melted, enhances the physical contact of LCO with LLZONb and further facilitates conduction of Li^+ ions between LCO and LLZO. The key is to use an interphase that is ionically conducting, electrochemically stable and wets both LLZO and LCO. This is not possible by using a sintering additive like LBO. Recently, an extremely low interfacial resistance was achieved by thermally soldering LCO and LLZO together. This was done by using $Li_{2.3-x}C_{0.7+x}B_{0.3-x}O_3$ (LCBO) that is formed by reaction between $Li_{2.3}C_{0.7}B_{0.3}O_3$ solder and the Li_2CO_3 coating (Fig. 8a)[94]. Li_2CO_3 is a spontaneously formed coating on surface of LLZO and LCO. $Li_{2.3}C_{0.7}B_{0.3}O_3$ powder was obtained by annealing Li_2CO_3 and LBO in air at 650 °C for 10 h. The $Li_{2.3}C_{0.7}B_{0.3}O_3$ was added into the cathode composite that reacts with Li_2CO_3 forming a conformal coating on both LCO and LLZO (Fig. 8b-d). The LCBO interphase has a much higher ionic conductivity compared to LBO and has excellent wetting properties. The slurry of cathode composite was coated on top of LLZO and annealed at 700 °C for 1 h in air. The LCBO enabled complete separation between LCO and LLZO which suppressed the elemental diffusions and chemical reactions leading to its superior chemical stability. An all-solid-state Li/LLZO/LCO battery fabricated by implementing this approach demonstrated excellent cycling performance and stability with room temperature capacity of 94 $mAhg^{-1}$ at 0.05 C for 100 cycles (Fig. 8e) and initial reversible capacity of 106 $mAhg^{-1}$ at 1C at 100 °C.
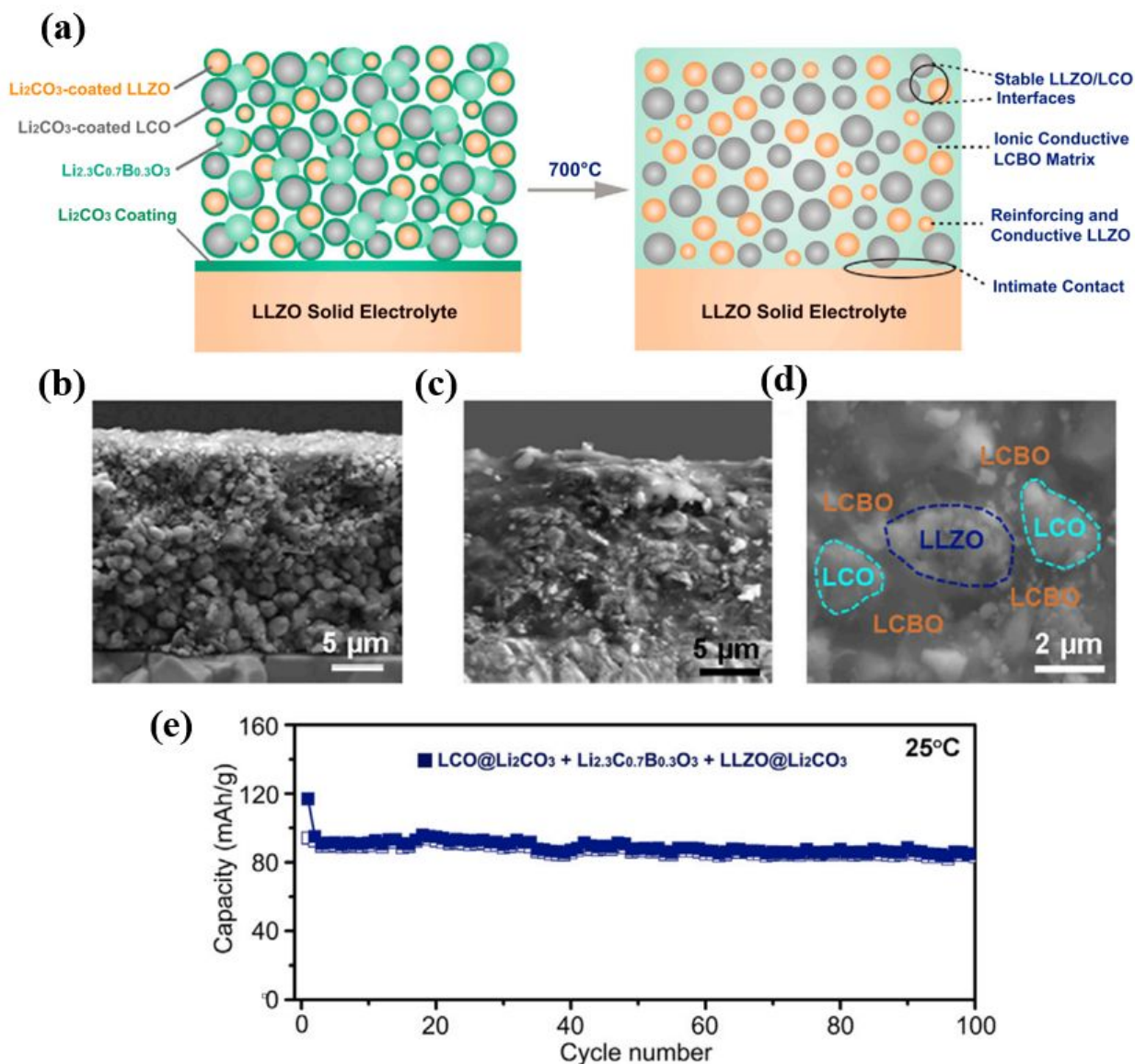
Fig. 8 LCBO interphase-modified all-ceramic lithium battery. (a) schematic showing the engineered all-ceramic cathode/electrolyte interface; Cross-sectional SEM images of the cathode composite ($Li_{2.3}Co_{0.7}B_{0.3}O_3$ + LLZO@Li_2CO_3 + LCO@Li_2CO_3) coated on LLZO (b) before sintering and (c) after sintering at 700 °C; (d) cross-sectional SEM image at high magnification of the cathode composite after sintering at 700 °C; (e) Cycling capacity of the all solid-state interface-engineered Li/LLZO/LCO cell at 0.05 C at room temperature. Reproduced with permission from Ref [94]. Copyright (2018) Cell Press.

Liu and coworkers found that doping Ta ions in LLZO could effectively enhance the ionic conductivity of the LLZO electrolyte[95]. 2.5 at% of Ta^{5+} ions were doped into the LLZO, which provided the ionic conductivity of $\sim 10^{-3}$ Scm^{-1}. LBO was employed in the cathode layer to provide good interfacial contact to assemble an all-solid-state battery. Maximum specific discharge capacity of 101.3 $mAhg^{-1}$ at room temperature was obtained. A cohesive and highly conductive polymer electrolyte employed in cathode layer or inserted in the interface of

electrolyte/anode achieved a three-dimensional ionic conductive network in the cathode layer and superior interfacial contact of the electrolyte/electrodes (Fig. 9a)[96]. As shown in the Fig. 9b-d, the SEM image of screen-printed cathode shows fluffy structure with uneven thickness, while the doctor bladed layers using PEO or PVdF as binder show more dense structure with uniform thickness. The electrochemical impedance spectroscopy (EIS) measurements of cathode/LAGP/cathode symmetrical cells as shown in Fig. 9e-g show that the impedance values for screen-printed LiFePO$_4$ (LFP) cathode is almost 200 times of that with PEO at 60 °C (15380 Ωcm^2 v/s 77 Ωcm^2) and 5 times when compared to cathode with PVdF in it at 60 °C (~15380 Ωcm^2 v/s 2690 Ωcm^2). Consequently, all-solid-state battery LiFePO$_4$/Li employing NASICON-type ionic conductor covered with PEO-based polymer exhibits excellent interfacial compatibility, ultra-long cycle life with high reversible discharge capacity maintained at 127.8 mAhg^{-1} for the 1000th cycle at 1 C (Fig. 9h), along with a retention of 96.6%, and an initial discharge capacity of 153.4 mAhg^{-1} with a high retention of 99.9% after 200 cycles at 0.1 C. Similarly, Zha et al. proposed LLZO-based membrane electrolyte where small amount of polymer binder was used to bind the LLZO particles[97]. The LLZO-based electrolyte layer was coated on top of cathode and was hot pressed to compact the structure of the electrolyte/cathode. The ionic conductivity of LLZO-PEO (9:1) before hot press showed an ionic conductivity of 6.39x 10^{-4} mScm^{-1} at 30 °C while hot pressing improved the conductivity to 4.26x 10^{-3} mScm^{-1} at 30 °C and 2.17x10^{-2} mScm^{-1} at 60 °C. An all-solid-state Li/90LLZO-10PEO/LiFePO$_4$ battery exhibited good cycling performance with discharge capacity of 148.3 mAhg^{-1} at 0.1 C after 50 cycles at 60 °C and 96 mAhg^{-1} at 25 °C.

The solid-state electrolyte requirements of high modulus to block Li-dendrite formation at Li-metal anode side and flexibility for good interfacial contact at cathode side are the main bottlenecks for its application. Thus, solid-state electrolytes that can incorporate features of both solid polymer electrolyte and inorganic ceramic electrolyte which can mitigate or minimize the interface resistance and dendrite growth respectively is the current requirement to recognize an efficient all-solid-state battery. Duan et al. employed in situ polymerization technique to assemble a lithium metal battery based on an asymmetric solid electrolyte (ASE) [98]. A stack of cathode LiFePO$_4$, precursor solution of polymerization, LLZO-coated separator and Li metal anode was prepared and heated at 80 °C for 48 h to accomplish the polymerization process. The precursor solution consisted of polymer monomer poly(ethylene glycol) methyl ether acrylate/LiTFSI/heat initiator BPO. Thus, prepared ASE had Li-ion conductivity of 1x10^{-4} Scm^{-1} at 55 °C and wide electrochemical window up to 4.8 V. The SEM and EPMA-EDS analysis showed good adhesion of electrodes with electrolyte. The bulk resistance and charge transfer resistance of battery assembled with the ASE at 55 °C were 49.68 and 609.8 Ωcm^2, respectively which were lower than those of LFP/LLZTO/Li batteries. The LFP/ASE/Li battery showed high initial discharge capacity of 160.6 mAhg^{-1} and initial coulombic efficiency of 99.17% at 0.2 C and 55 °C.
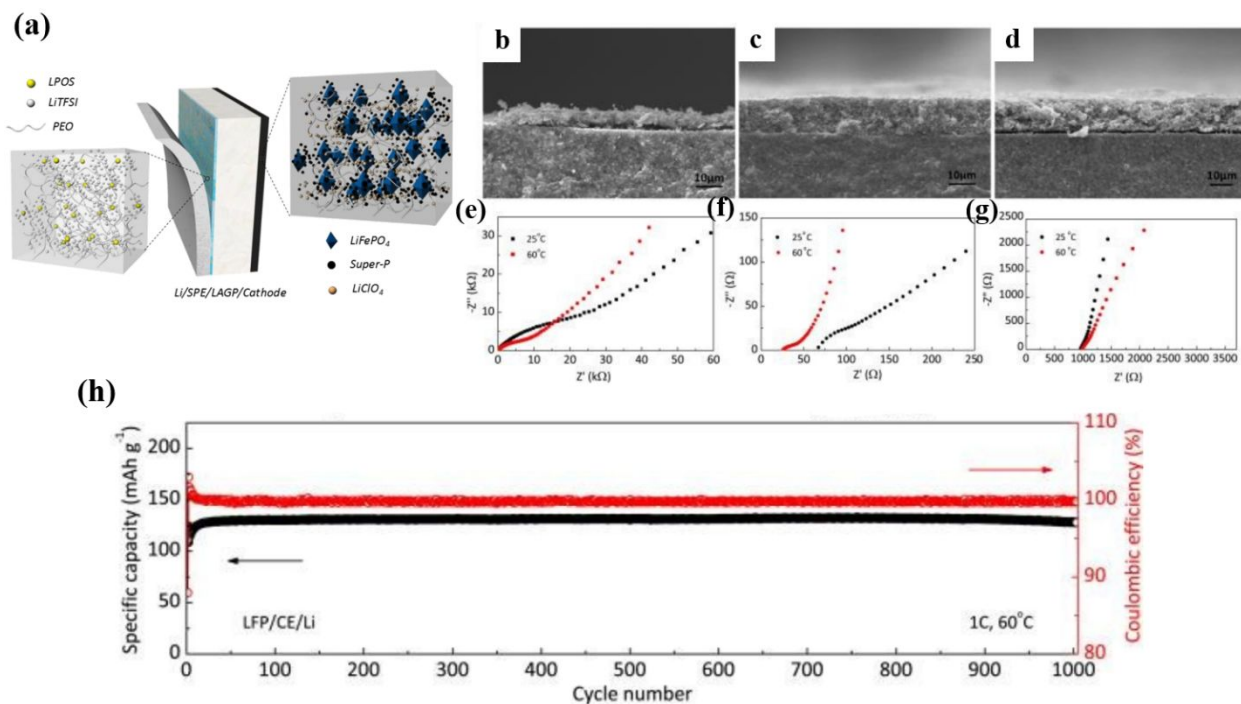
Fig. 9 Composite electrolyte based on coating of PEO-based solid polymer electrolyte on LAGP pellets. (a) Schematic showing an all-solid-state Li/composite electrolyte/LiFePO$_4$ cell; Cross-sectional SEM images of the LAGP/LFP interface prepared by (b) screen printing, (c) doctor-blade with PEO, and (d) doctor-blade with PVDF; Nyquist plots of the cathode/LAGP/cathode symmetrical cells for which cathode was prepared by (e) screen printing, (f) doctor-blade with PEO and (g) doctor-blade with PVDF; (h) Long term cycling performance of all-solid-state Li/composite electrolyte/LiFePO$_4$ cell at 1C, 60 °C. Reproduced with permission from Ref [96]. Copyright (2017) Royal Society of Chemistry.

3.2.4. Surface coating

Modifying the interface by a suitable coating layer is another successfully demonstrated technique. Kato et al. introduced a thin Nb layer (~ 10 nm) on both sides of the LLZO pellet by RF sputtering and subsequently deposited LCO on the Nb-modified surface by PLD (Fig. 10a)[99]. The Nb-deposited LLZO pellet was heated at 873 K for 2h in O$_2$ environment. The introduction of the Nb layer leads to the formation of a Li$^+$ conductive amorphous phase at LLZO/LCO interface. This Li-Nb-O amorphous layer fulfills two purposes i) prevents cross diffusion of La and Co and formation of non-Li$^+$ conductive phase such as La$_2$CoO$_4$ and ii) fills the voids between LLZO and LCO. This led to a decrease in interfacial resistance from 2600 Ωcm^{-2} to 150 Ωcm^{-2} (Fig. 10b) and high rate capability of Li/LLZO/LCO all-solid-state battery (Fig. 10c). Wang et al. reported a unique and effective mixed ionic-electronic (MIE) conducting cathode-garnet interface which showed enhanced Li transport after slow pre-lithiation[100]. The TiS$_2$ and P3-CNTs were sonicated and dispersed in N-Methyl-2-pyrrolidone (NMP) solvent and coated on garnet solid state electrolyte (SSE). The carbon nanotubes provide channels for global electron transport whereas TiS$_2$ assists in local electron transport in the design. After pre-lithiation process, the layered TiS$_2$ structure enhances the Li ion transport. Variation in EIS

spectra according to temperature was observed for solid-state batteries. As the temperature was varied from 60 °C to 150 °C, the electrolyte/electrode interfacial resistance decreased from more than 6000 Ωcm^2 to less than 100 Ωcm^2.
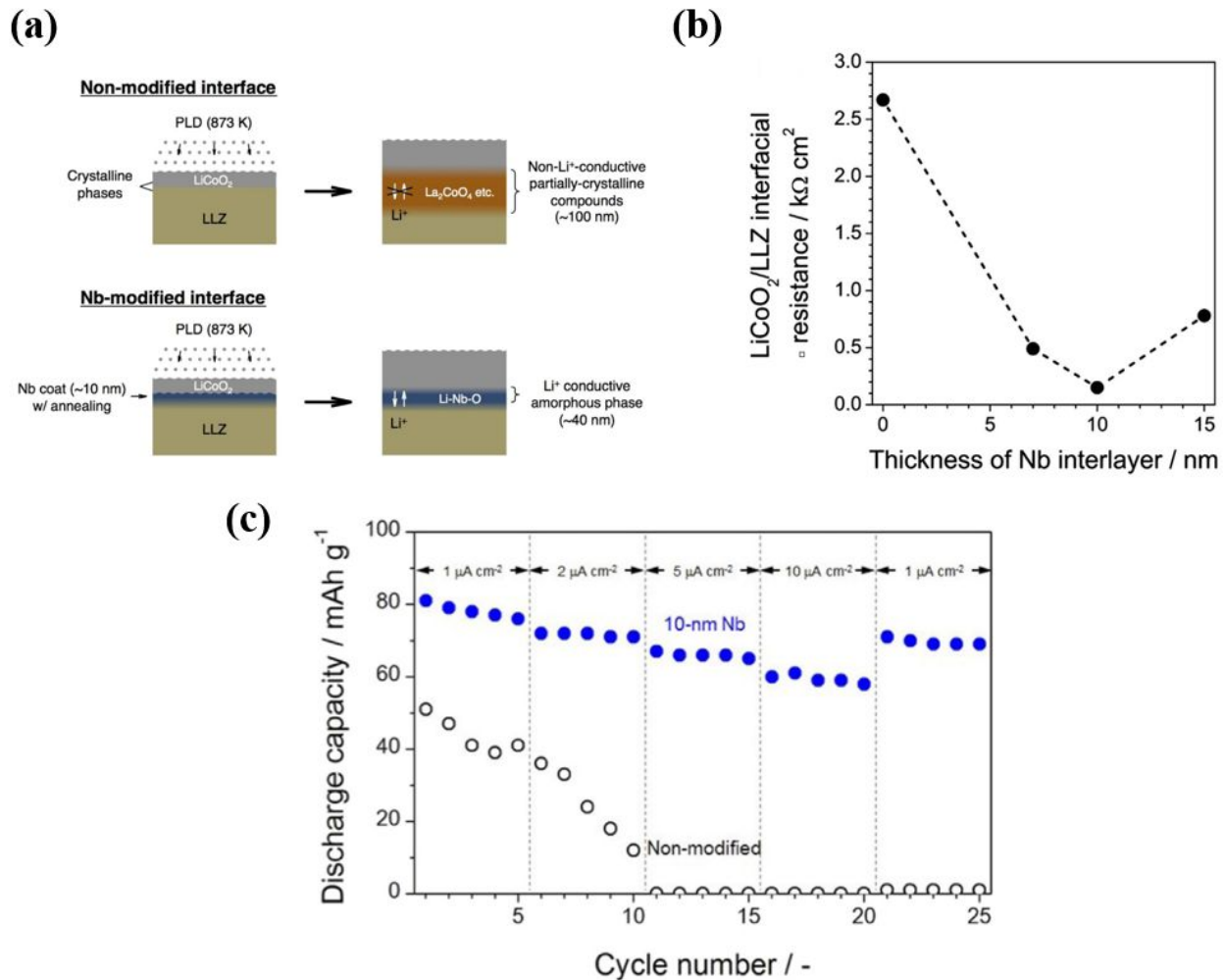
Fig. 10 Surface modification using Nb. (a) schematic of the approach; (b) Interface resistance as a function of Nb layer thickness; (c) Rate capability curves comparing the Nb-modified Li/LLZO/LCO cells vs non-modified. Reproduced with permission from Ref [99]. Copyright (2014) Elsevier.

3.2.5. Porous garnet interface structure

An interesting technique was reported which utilizes porous interface of garnet electrolyte that can facilitate intimate accommodation of the electrode material into the garnet electrolyte (Fig. 11a)[101]. A sacrificial organic template was employed on dense c-Li$_{6.25}$Al$_{0.25}$La$_3$Zr$_2$O$_{12}$ pellets which on sintering at high temperature at 1075 °C under an O$_2$ rich environment resulted into a porous interface. The LTO electrode slurry consisting of LTO, c-Li$_{6.25}$Al$_{0.25}$La$_3$Zr$_2$O$_{12}$ powder, conductive carbon and PVDF binder was then casted on to the thus formed porous pellet surface. The casted electrode is intimately embedded into the pores of the pellet, in contrast to the flat pellet and electrode interface for the non-modified cell (Fig. 11b). The interface engineered all

solid-state battery showed significant decrease in resistance (Fig. 11c) and thus exhibited higher discharge capacity compared to the non-modified battery (Fig. 11d).
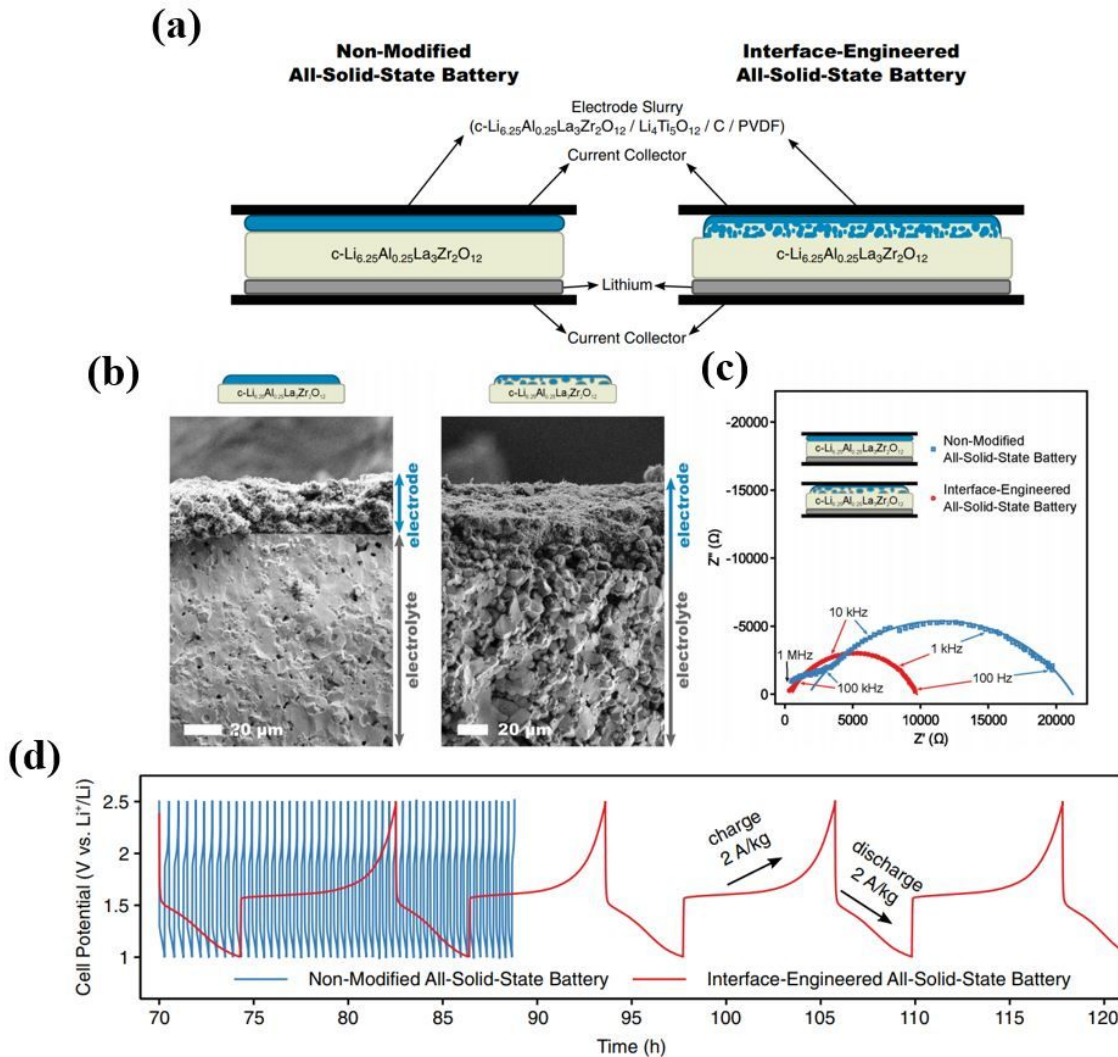

Fig. 11 Porous interface of c-$Li_{6.25}Al_{0.25}La_3Zr_2O_{12}$ garnet structure. (a) Schematic showing non-modified and modified interfaces; (b) experimental approach to obtain the porous interface on dense pellets; (c) Cross-sectional SEM images of the interface of the pellet with LTO; (d) Nyquist plots of all-solid-state cells with LTO and Li metal electrodes with non-modified and modified interface; (e) Charge/discharge voltage profiles of the non-modified and interface engineered all-solid-state cells. Reproduced with permission from Ref [101]. Copyright (2016) John Wiley and Sons.

3.2.6. Plastic crystal interlayer

Lu et al. employed plastic crystal interlayer which are based on succinonitrile with a fluoroethylene carbonate additive to modify the electrode|Ta-doped-LLZO (LLZTO) interface and enhance Li^+ ion transport in it (Fig. 12a-e) [102]. The area-specific resistance (ASR) at the interface for Li|LLZTO|$LiFePO_4$ battery dropped from ~13,000Ωcm^2 to ~560Ωcm^2 after coating the interlayer. This interlayer incorporated battery can cycle over 50 cycles maintaining capacity

23

of 140 mAhg^{-1} at room temperature (Fig. 12f). Further, the total drop in resistance for Li symmetrical cells was by factor of 16 between coated (~100 Ωcm^2) and uncoated cell (~1600 Ωcm^2).
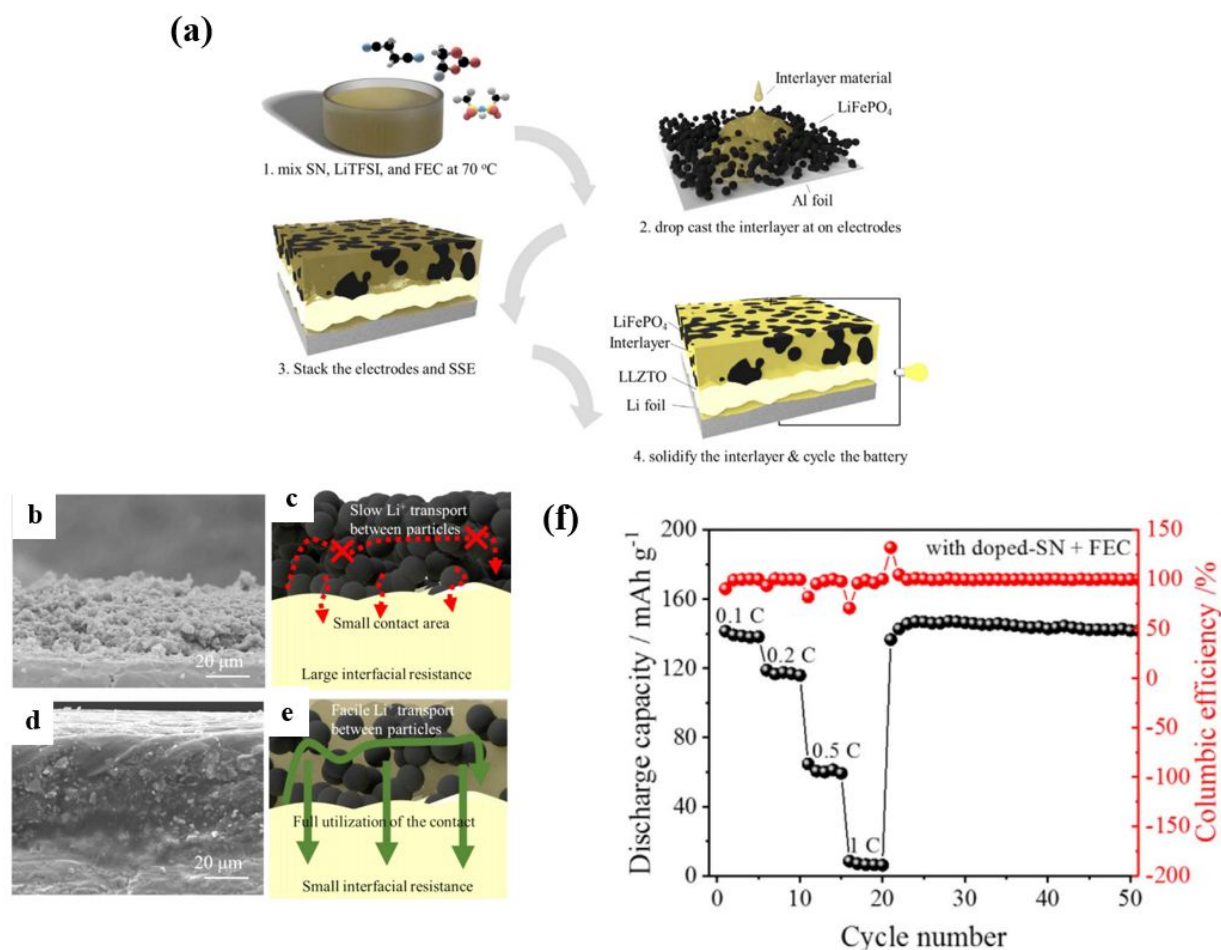
Fig. 12 Plastic crystal interlayer based on succinonitrile (SN) with fluoroethylene carbonate (FEC) additive. (a) Schematic of interlayer preparation; Cross-sectional SEM images of LiFePO$_4$/LLZTO interface (b) without and (d) with interlayer; Schematic showing Li$^+$ transport at the LiFePO$_4$/LLZTO interface (c) without and (e) with interlayer; (f) Rate capability of the all-solid-state Li./LLZTO/LiFePO$_4$ cell with SN+FEC as interlayer. Reproduced with permission from Ref [102]. Copyright (2019) Elsevier.

3.3. Lithium/Sulfide electrolyte interface

Most sulfide electrolytes with high ionic conductivity are chemically unstable with lithium metal. This interface instability leads to formation of lithium dendrites along the voids and grain boundaries in these sulfide electrolytes. The decomposition products at the interface have much lower ionic conductivity and higher electronic conductivity, thus making the interphase vulnerable to lithium dendrite growth as well. One of the strategies to reduce the electrochemical reduction of sulfide electrolytes has been the use of lithium alloys with a higher lithiation/delithiation potential[103]. However, this lithium alloy significantly compromises the maximum cell energy density that the lithium metal anode can deliver. Therefore, it is critical to

24

find alternative approaches to address this interfacial instability in order to realize the use of sulfide electrolytes with lithium metal. Several promising approaches have been applied which are further discussed.

3.3.1. Surface coating

Tatsumisago et al. modified the interface of Li_2S-P_2S_5 sulfide solid electrolyte by inserting an Au thin film between the electrolyte and Li metal via thermal evaporation[104]. The use of this Au film helped to achieve a higher utilization of Li metal with galvanostatic cycling of the symmetrical cells compared to that without the Au film. Similarly, the group studied insertion of an indium thin layer in between Li and Li_2S-P_2S_5 sulfide solid electrolyte[105]. Lithium-indium alloy possesses a high lithium ion diffusion coefficient. The deposition of the indium layer demonstrated good cyclability and rate capability for Li/LTO solid state cells. Similarly, Xu et al. introduced an in situ formed LiH_2PO_4 protective layer on Li metal surface by spin casting different concentration of phosphoric acid solution in THF[106]. This protective layer improves the chemical stability of LGPS to Li metal by preventing the migration of mixed ionic-electronic reactants into the LGPS, thus limiting the interphases. Symmetrical cell showed low overpotential with cycling over 950 h at 0.1 mAcm^{-2}. Further, a solid-state cell based on LCO/LGPS/Li with the engineered interface demonstrated excellent cycling performance with 131.1 and 113.7 mAhg^{-1} for the 1st and 500th cycle respectively.

　　Aliovalent substitution of Li_4SnS_4 to form $Li_{3.833}Sn_{0.833}As_{0.166}S_4$ solid electrolyte that has a higher ionic conductivity of 1.39 mScm^{-1} at room temperature as well as excellent air stability was reported[107]. However, this modified sulfide electrolyte was also unstable or compatible with metallic Li electrode. To address this, the surface of the solid electrolyte was chemically passivated with a Li-compatible composite of $3LiBH_4$.LiI in THF solvent. This surface modification led to a stable cycling of the symmetrical cells, demonstrating the compatibility of the passivated electrolyte with the metallic lithium. Xu et al. introduced a combination of two approaches to prevent the growth of Li dendrites, namely, i) LiF or LiI interface layer between Li and sulfide electrolyte and ii) methoxyperfluorobutane (HFE) (or I solution) to penetrate into the solid sulfide electrolyte (Fig. 13a)[103]. In addition to the dendrite suppression facilitated by the LiF or LiI interface layer, the infiltrated HFE (or I) in the sulfide electrolyte can consume the lithium dendrites forming LiF (or LiI), thus forming a stable and compatible interface of sulfide electrolyte with lithium (Fig. 13b). The interface modified Li symmetrical cells exhibited much lower interfacial impedance compared to the non-modified cells (Fig. 13c). An all-solid-state lithium battery of $LiNbO_3$ coated $LiCoO_2$/$Li_7P_3S_{11}$/Li was assembled with HFE infiltrated sulfide electrolyte and LiF coated Li metal which demonstrated reversible capacity of 118.9 mAhg^{-1} and retention of 96.8 mAhg^{-1} after 100 cycles (Fig. 13d).
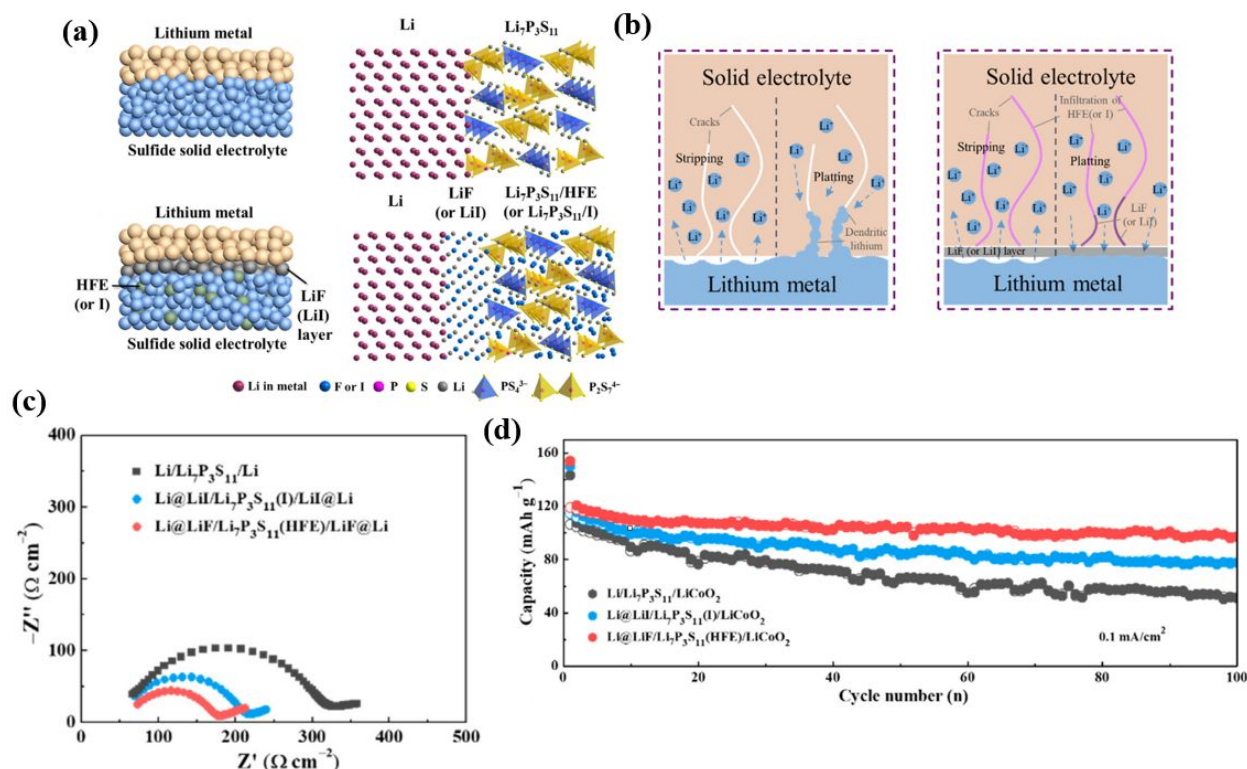
Fig. 13 Interface engineering using LiF (or LiI) interphase layer and HFE (or I solution) infiltrated sulfide electrolyte. (a) Schematic showing the interface modification; (b) Schematic showing lithium stripping/plating process of bare and interface modified Li metal; (c) Nyquist plots of Li symmetrical cells based on pristine and interface modified $Li_7P_3S_{11}$ sulfide electrolyte; (d) Cycling performance of LCO-based all-solid-state battery using without and with interface modification at 0.1 mAcm^{-2} at 25 °C. Reproduced with permission from Ref [103]. Copyright (2018) Elsevier.

Wang et al. introduced use of molecular layer deposition (MLD) to deposit an inorganic-organic hybrid interlayer (alucone) on lithium metal surface as an artificial SEI layer[108]. The 30 MLD cycles alucone coating on Li metal displayed almost stable interfacial resistance with total minimum resistance compared to bare Li metal, suggesting suppression of interfacial reactions at the interface between $Li_{10}SnP_2S_{12}$ sulfide electrolyte and Li metal. Longer cycling was exhibited for plating/stripping process of Li symmetrical cells by the 30 MLD cycles alucone coated Li metal in comparison to bare Li. Further, an all-solid-state cell using this modified Li metal delivered a high initial capacity of 120 mAhg^{-1}, retaining 60 mAhg^{-1} after 150 cycles. Similarly, an efficient technique to stabilize the Li/LGPS interface by modifying surface of the lithium electrode with a nanocomposite interphase consisting of organic (LiO-(CH2O)n-Li) and inorganic (LiF, -NSO2-Li, Li2O) salts was demonstrated by Guo et al. (Fig. 14a,b)[109]. This interphase was developed by in situ electrochemical reduction of a liquid electrolyte on the Li metal. This interphase can serve as an interfacial protective layer facilitating prevention of LGPS reduction by Li during cycling and thus stabilizing the Li/LGPS interface. Further, this interphase also enables fast ion conduction at the interface. Using this interphase, Li/LGPS/Li

symmetrical cell demonstrated cycling of over 3000h (Fig. 14c) and Li/LGPS/TiS$_2$ full cell achieved improved cycling stability over 200 cycles compared to bare Li (Fig. 14d).
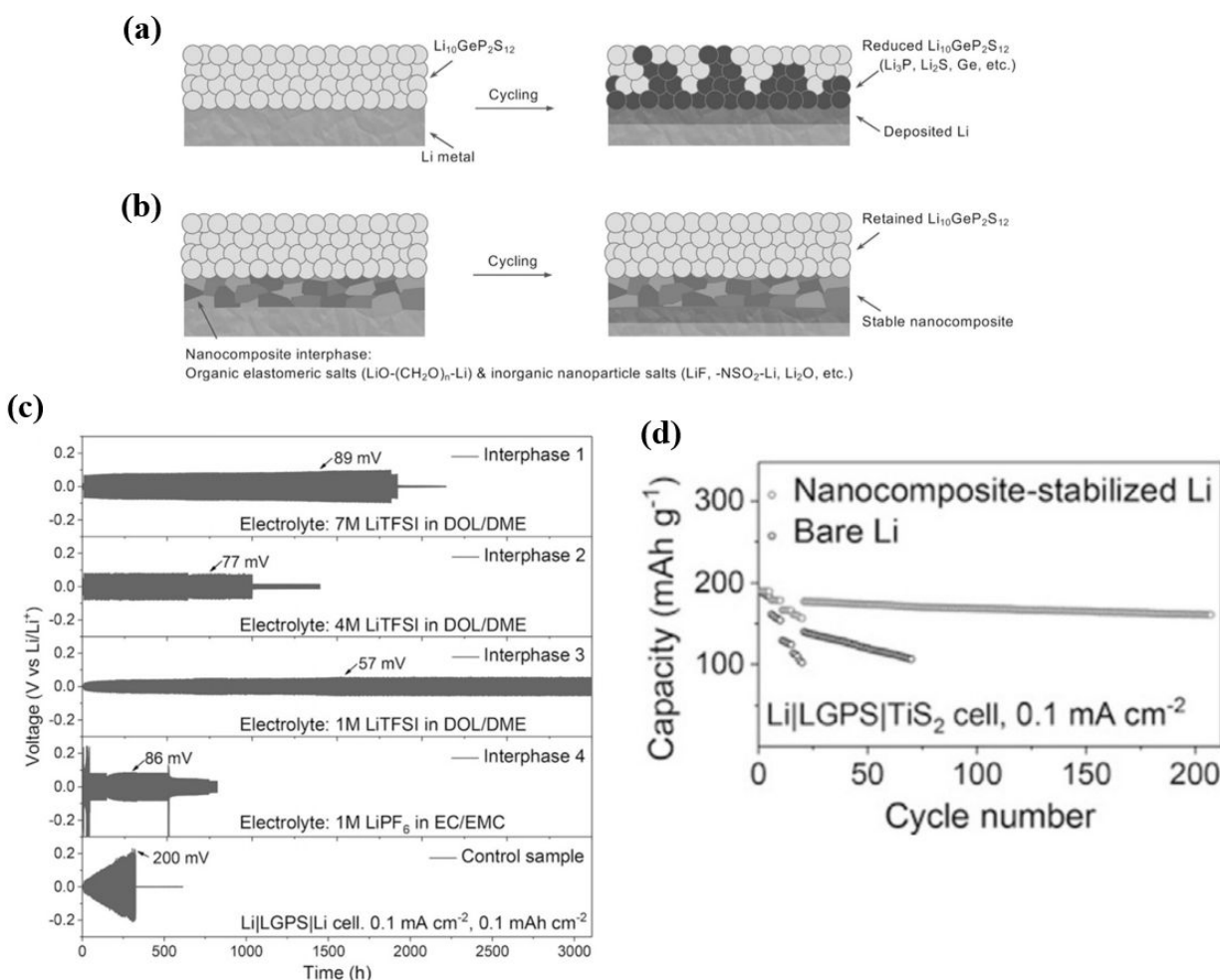
Fig. 14 Modification of lithium metal surface using Li salt-based organic-inorganic nanocomposite interphase. Schematics showing (a) poor interface and (b) stable interface between Li and LGPS; (c) plating/stripping voltage profiles of Li/Li symmetrical cells with different electrolyte compositions; (d) Cycling performance of all-solid-state Li/LGPS/TiS$_2$ full cells comparing bare Li and nanocomposite-stabilized Li. Reproduced with permission from Ref [109]. Copyright (2018) John Wiley and Sons.

Philip et al. introduced use of solvate coated sulfide electrolytes using lithium bis(trifluoromethane sulfonyl)imide and a highly fluorinated ether solvate electrolyte[110]. Two thiophosphates namely, Li$_7$P$_3$S$_{11}$ (LPS) and LGPS were examined for this purpose. Different observations were observed for these two types of electrolytes. Cell resistance with time was found to decrease for solvate-LGPS (compared to LGPS) but increase for solvate-LPS (compared to LPS). This was attributed to solvate permeation into the bulk of LGPS. While LPS-1,1,2,2-tetrafluoroethyl 2,2,3,3-tetrafluoropropyl ether (TTE) layer was formed on the surface of LPS pellet, attributed to its higher solubility in TTE. Cyclic voltammetry tests showed much

enhanced current density for solvate-LGPS compared to LGPS, while the solvate-LPS showed much better cycling stability (100 cycles) versus LPS (2 cycles).

3.3.2. Elemental Substitution/Doping

Despite the highest ionic conductivity displayed by sulfide solid electrolytes such as LGPS, its structural stability needs to be improved, which will further improve the electrochemical stability against Li metal. Yang et al. reported partially substituting Li sites by divalent Ba metal ions to realize high structural stability of LGPS[111]. It was observed that $Li_{0.9}Ba_{0.3}GeP_2S_{12}$, although demonstrates a lower ionic conductivity of 7.04×10^{-4} Scm^{-1} vs LGPS with 1.43×10^{-3} Scm^{-1}, the symmetrical cells with the modified LGPS demonstrated much reduced polarization. This further implied the enhancement in structural stability of LGPS owing to the strong coulombic interaction between Ba^{2+} and S^{2-} sites as was indicated by the blue shift observed in Raman spectra. Better thermodynamic stability is expected, with chemical bonds between Ge/P-O being stronger than the Ge/P-S. With this in view, Sun et al. partially substituted sulfur by oxygen to form oxysulfide $Li_{10}GeP_2S_{12-x}O_x$ solid electrolyte[112]. It was confirmed that the oxygen substitution takes place at S(1) positions leading to local structural change in the PS_4 tetrahedra. High ionic conductivities of 1.03×10^{-2} to 8.43×10^{-2} Scm^{-1} were observed for $Li_{10}GeP_2S_{11.7}O_{0.3}$ and $Li_{10}GeP_2S_{11.4}O_{0.6}$ systems vs the LGPS with 1.02×10^{-2} Scm^{-1} along with excellent electrochemical stability in voltage range of 0-10 V vs Li/Li^+. All solid-state cells based on $LiNbO_3$ coated LCO/Li with the modified LGPS solid electrolyte showed better cycling performance compared to LGPS.

Xu et al. introduced MoS_2 doped $Li_2S-P_2S_5$ glass ceramic sulfide solid electrolyte produced by high energy ball milling and annealing[113]. The doped sulfide electrolyte $Li_7P_{2.9}S_{10.85}Mo_{0.01}$ maintained the structure of the $Li_7P_3S_{11}$ sulfide family and delivered higher ionic conductivity of 4.8 $mScm^{-1}$ at room temperature vs $Li_7P_3S_{11}$ (Fig. 15a,b). Further, $Li_7P_{2.9}S_{10.85}Mo_{0.01}$ exhibited better compatibility with lithium metal with lower interfacial impedance and significantly suppressed side reactions in the voltage range of 4-5 V (vs Li/Li^+) compared to the $Li_7P_3S_{11}$ (Fig. 15c-e). This led to better cycling performance of all-solid-state Li-S batteries based on the doped sulfide electrolyte with discharge capacity of 1020 $mAhg^{-1}$ compared to the $Li_7P_3S_{11}$ with 775 $mAhg^{-1}$ (Fig. 15f). While, Liu et al. introduced aliovalent substitution of Li_3PS_4 sulfide electrolyte by Zn, O co-doping using 2 mol% ZnO, where Zn^{2+} substitutes partial P^{5+} and O^{2-} substitutes partial S^{2-}.[114] In addition to the structural stability and high ionic conductivity of 1.12×10^{-3} Scm^{-1} at room temperature (Fig. 16a,b), the thus developed $Li_{3.06}P_{0.98}Zn_{0.02}S_{3.98}O_{0.02}$ sulfide electrolyte also demonstrated excellent stability against lithium metal as well as in air (Fig. 16c). An all-solid-state cell using bilayer electrolytes with $LiCoO_2/Li_{10}GeP_2S_{12}/Li_{3.06}P_{0.98}Zn_{0.02}S_{3.98}O_{0.02}/Li$ (as shown in Fig. 16d) showed an initial capacity of 139 $mAhg^{-1}$ at 0.1 C with a retention of 81.0% after 100 cycles at room temperature compared to $LiCoO_2/Li_{10}GeP_2S_{12}/Li_3PS_4/Li$ cell with 127.7 $mAhg^{-1}$ with 37.7% retention after 60 cycles (Fig. 16e). Similarly, sulfur substitution by oxygen in argyrodite sulfide solid electrolyte Li_6PS_5Br where, O atoms substituted S atoms at the free S^{2-} sites rather than at PS_4 tetrahedra was reported by Zhang et al.[115]. The O-doped $Li_6PS_{4.7}O_{0.3}Br$ solid sulfide electrolyte showed better electrochemical and chemical stability against metallic lithium than Li_6PS_5Br.

Further, all-solid-state cells comprising of NCM-811/$Li_6PS_{4.7}O_{0.3}Br$/Li-In exhibited enhanced capacities and rate capability compared to NCM-811/Li_6PS_5Br/Li-In.
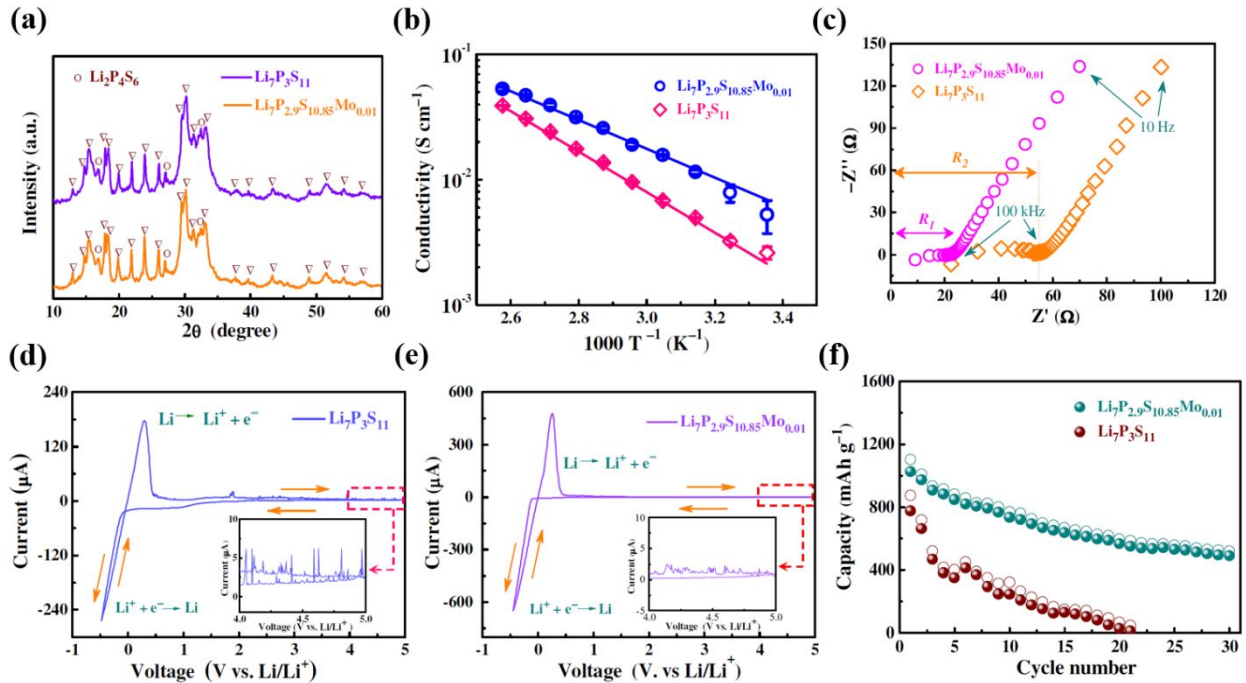
Fig. 15 MoS$_2$ doping of Li_2S-P_2S_5 glass-ceramic electrolyte. (a) XRD patterns (b) Arrhenius conductivity plots (c) Nyquist plots of $Li_7P_3S_{11}$ and $Li_7P_{2.9}S_{10.85}Mo_{0.01}$; Cyclic voltammetry curves of Li symmetrical cells employing (d) $Li_7P_3S_{11}$ and (e) $Li_7P_{2.9}S_{10.85}Mo_{0.01}$, (Inset shows modified view between 4-5 V); (f) Cycling performance of all-solid-state Li-S batteries using $Li_7P_3S_{11}$ and $Li_7P_{2.9}S_{10.85}Mo_{0.01}$ at C/20 at room temperature. Reproduced with permission from Ref[113]. Copyright (2017) Royal Society of Chemistry.
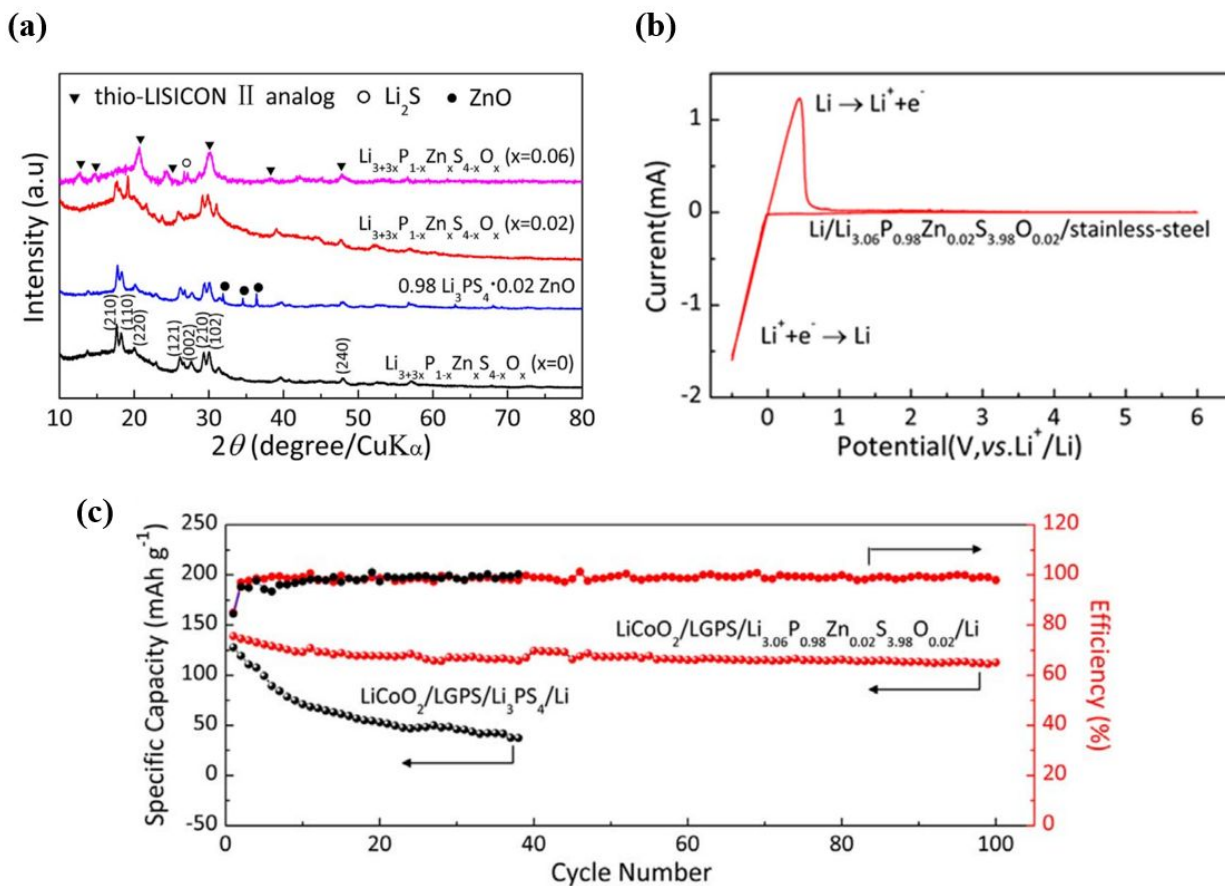
Fig. 16 ZnO-doped Li_3PS_4 sulfide electrolyte. (a) XRD patterns of $Li_{3+3x}P_{1-x}Zn_xS_{4-x}O_x$ ad $0.98Li_3PS_4-0.02ZnO$; (b) Cyclic voltammetry curve of $Li_{3.06}P_{0.98}Zn_{0.02}S_{3.98}O_{0.02}$ in potential range of -0.5V to 6 V (vs Li/Li$^+$); (c) Cycling performance of the all-solid-state cell based on the doped and undoped Li_3PS_4 at 0.1 C at room temperature. Reproduced with permission from Ref [114]. Copyright (2019) Elsevier.

Lu et al. added Li_2ZrO_3 as a dopant to $70Li_2S-30P_2S_5$ glass ceramic sulfide electrolyte to obtain a series of $(100-x)(70Li_2S-30P_2S_5)-xLi_2ZrO_3$ (x = 0, 1, 2, 5), where 1 mol% of Li_2ZrO_3 was found to be the optimum amount[116]. The $99(70Li_2S-30P_2S_5)-1Li_2ZrO_3$ demonstrated higher ionic conductivity of 2.85×10^{-3} Scm^{-1} at room temperature compared to the pristine $Li_2S-P_2S_5$ with 1.65×10^{-3} Scm^{-1}. An all-solid-state battery employing the modified electrolyte demonstrated higher discharge capacities by 21.9% for the 50th cycle and lower interfacial resistance between the electrodes and the solid electrolyte, which was attributed to the high lithium ion diffusion coefficient and stable crystal structure of Li_2ZrO_3. Tatsumisago's group reported use of P_2O_5 to prepare $70Li_2S \cdot (30 - x)P_2S_5 \cdot xP_2O_5$ (mol%) oxysulfide glass ceramics, prepared by melt quenching method where the glass ceramics were heated at temperature above the crystallization temperature[117-119]. The oxysulfide glass ceramic exhibited higher ionic conductivity and improved electrochemical stability. Tao et al. reported similar P_2O_5 doping of the $75Li_2S \cdot 25P_2S_5$ sulfide solid electrolyte, prepared by mechanical milling and heating[120]. An enhanced ionic conductivity of 8×10^{-4} Scm^{-1} at room temperature was observed for

$75Li_2S \cdot 24P_2S_5 \cdot 1P_2O_5$ electrolyte. Cyclic voltammetry tests showed that the lithium deposition/dissolution reactions take place at 0-0.5 V range, while no peaks were observed in 0.5-10 V range, indicating the compatibility of the electrolyte with metallic lithium. Further, lithium symmetrical cell tests indicated lower polarization for the $75Li_2S \cdot 24P_2S_5 \cdot 1P_2O_5$ electrolyte compared to pristine $75Li_2S \cdot 25P_2S_5$, further demonstrating its compatibility with metallic lithium. All-solid-state Li battery with $LiCoO_2/75Li_2S \cdot 24P_2S_5 \cdot 1P_2O_5$ delivered a higher discharge capacity of 109 mAhg^{-1} at 0.1 C with retention of 85.2% after 30 cycles compared to the pristine $75Li_2S \cdot 25P_2S_5$ electrolyte with 84.6 mAhg^{-1} at 76.2% retention.

Similarly, Sb_2O_5 doping of Li_3PS_4 sulfide electrolyte was studied with a series of $Li_3P_{1-x}Sb_xS_{4-2.5x}O_{2.5x}$ electrolytes prepared by high energy ball milling followed by heat treatment[121]. Among the several electrolytes studied, the $Li_3P_{0.98}Sb_{0.02}S_{3.95}O_{0.05}$ ($x = 0.02$) showed the highest ionic conductivity of 1.08 mScm^{-1} compared to Li_3PS_4 with 0.5 mScm^{-1}. In addition, the doped electrolyte also exhibited no reactions up to 5 V, except the lithium deposition and dissolution reactions under 0.5 V. For lithium symmetrical cell tests, the doped electrolyte showed superior stability with steady voltage profiles compared to the pristine electrolyte. All-solid-state batteries with $LiCoO_2$/bilayer electrolyte $Li_{10}GeP_2S_{12}$/doped or pristine Li_3PS_4/Li showed much higher discharge capacity of 133.7 mAhg^{-1} at 0.1 C for the doped electrolyte compared to pristine with 127.7 mAhg^{-1}. In addition, much faster capacity fading was observed with the pristine electrolyte which demonstrated a retention of 36.1% after 50 cycles, while the doped electrolyte retained 78.6%. This can be ascribed to the side reactions at the Li_3PS_4/Li interface that form Li_2S layer.

Transition metal phosphides have been explored as anode materials for battery applications owing to their high conductivity, low polarization and low volume change during cycling. The Li_3P formed after Li intercalation into the metal phosphide has high Li$^+$ conductivity and lithium metal stability. With this into consideration, Ge et al. investigated the doping of $Li_7P_3S_{11}$ using Ni_2P[122]. Among the series of electrolyte (100-x) $(70Li_2S-30P_2S_5)$-xNi_2P ($x = 0, 1, 2, 3, 4$) tested, $Li_7Ni_{0.2}P_{3.1}S_{11}$ exhibited the highest ionic conductivity of 2.22 mScm^{-1} at room temperature, 1.6 times higher than the pristine $Li_7P_3S_{11}$. A more smoother CV curve for the $Li_7Ni_{0.2}P_{3.1}S_{11}$ depicted that the presence of Ni_2P has better compatibility with the lithium electrode. An all-solid-state Li-S battery was fabricated with Li_2S as anode which demonstrated initial discharge capacity of 429 mAhg^{-1} at 0.064 mAcm^{-2} and 454 mAhg^{-1} after 20 cycles.

3.3.3. Solution processed sulfide electrolytes

Finding a facile, efficient and cost-effective method to form the solid electrolytes is crucial. A liquid based synthesis and processing route can be one of the methods. It is important that the solvent used during the processing is not reactive towards the Li metal. With this into consideration, Liu et al. demonstrated synthesis of thin film Li_3PS_4 sulfide electrolyte by solution processing[123]. This involved casting a β-Li_3PS_4 solution on to Li metal that was formed by reaction between soluble polysulfides and P_2S_5 in diethylene glycol dimethyl ether solvent. A thin and dense solid electrolyte with a high-quality interface with Li metal was formed. Excellent electrochemical stability against Li metal and stable cycling of symmetrical cells was observed.

3.3.4. Hybrid of sulfides with polymer

A hybrid of solid sulfide electrolyte $Li_7P_3S_{11}$ (LPS) with polymer composite of polyethylene oxide-$LiClO_4$ was demonstrated by Xu et al. (Fig. 17a)[124]. The polymer not only was able to facilitate Li^+ transport between the sulfide electrolyte particles and increase the ionic conductivity, but also suppress the reaction between metallic lithium and the sulfide electrolyte by isolating the two (Fig. 17c,d). This enabled a Li-S battery using the hybrid electrolyte (Fig. 17b) to achieve a much better cycling stability with discharge capacity of 394 mAhg^{-1} after 60 cycles and retention of 47.7% in comparison to the LPS electrolyte with only 6.1 mAhg^{-1} and 0.8% retention (Fig. 17e). Likewise, Zhang et al. introduced a hybrid of argyrodite sulfide electrolyte Li_6PS_5Cl with poly(ethylene oxide) (PEO) to address poor mechanical strength of the electrolyte and its unstable interface with lithium[125]. Although the pristine Li_6PS_5Cl has the highest ionic conductivity, addition of the polymer was able to form a stable interface with lithium, attributed to the enhanced mechanical property of the sulfide electrolyte. No changes were observed in bulk of the electrolyte after cycling. While, the Li/sulfide electrolyte interface with 5 wt% PEO showed no new solid electrolyte layer formation, thus achieving lower variation of interfacial resistance after cycling. All-solid-state Li-S battery fabricated with $LiNi_{0.8}Co_{0.1}Mn_{0.1}O_2$ (NCM) as cathode and hybrid electrolyte with 5 wt% PEO exhibited superior capacity retention of 44% after 500 cycles compared to pristine Li_6PS_5Cl with 27%.
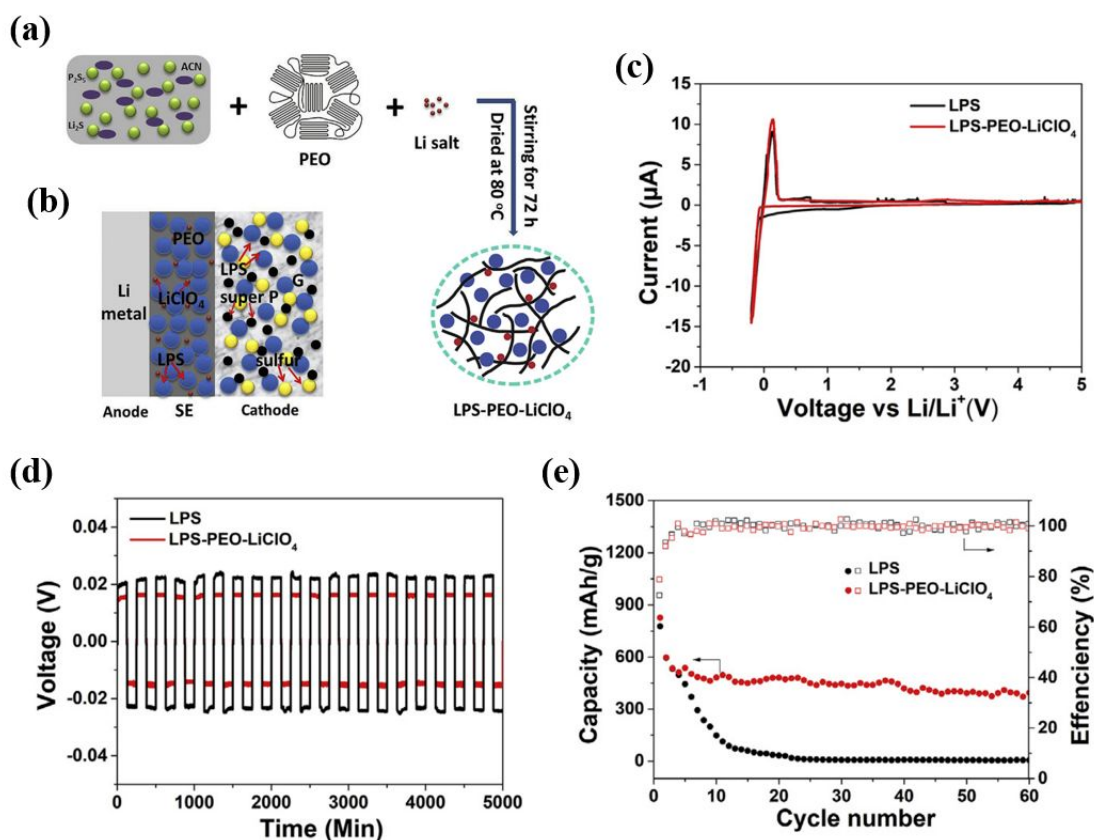
Fig. 17 Hybrid $Li_7P_3S_{11}$/PEO-$LiClO_4$ electrolyte. (a) Schematic showing composite preparation process; (b) Schematic of an all-solid-state Li-S cell based on the composite electrolyte; (c)

Cyclic voltammetry curves of Li/electrolyte/stainless steel cells; (d) Voltage profiles of Li-Li symmetrical cells based on the LPS and the composite electrolyte; (e) Cycling performance of all-solid-state Li-S cells based on LPS and the composite electrolyte. Reproduced with permission from Ref[124]. Copyright (2018) Elsevier.

3.4. Lithium/Oxide Electrolyte Interface

Among the solid-state electrolytes, garnet-type oxide electrolytes demonstrate the lowest reduction potential against the metallic lithium and the most thermodynamically stable interface with the lithium[126]. However, the rigid ceramic nature of the garnet-based solid-state electrolytes leads to the large interfacial impedance. A rather simple method to reduce the large interfacial resistance is addition of liquid electrolyte at the interface which is known as solid-liquid hybrid electrolyte interface. Wang et al. presented a quantitative analysis of required volume of liquid electrolyte (1M $LiPF_6$ in ethylene carbonate (EC)/ dimethyl carbonate (DMC)/ diethyl carbonate (DEC) with a volume ratio of 1:1:1) in the interface between electrode and $Li_{1.4}Al_{0.4}Ti_{1.6}(PO_4)_3$ (LATP) solid electrolyte pellet by measuring the interfacial properties of the thus prepared cells[127]. The analysis showed that interfacial resistance of the cell while using 1μL of the liquid electrolyte is about 1000 Ω whereas, increasing the liquid electrolyte volume to 2 μL leads to decrease of interfacial resistance to 275 Ω. However, addition of any amount of liquid electrolyte would compromise the merits of an all-solid-state battery.

The general practice of pressing Li foil into LLZO garnet pellets can be used for analyzing interfacial resistance, while adding heat during the pressing can further enhance the effectiveness of the process. Wang and Sakamoto tested Li|LLZO|Li symmetric cells and showed a strong relationship between the interfacial resistance and adhesive strength of Li-LLZO interface, σ_{adh}[128]. For the highest interfacial resistance of 330 kΩcm^2 in the study, σ_{adh} of 1.1 kPa was observed, while the lowest interfacial resistance of 7Ωcm^2 showed the σ_{adh} of 8MPa. The other approach is heating or melting of the lithium metal on top of the garnet electrolytes. However, this process leads to small microscopic gaps at the interface, which is due to the poor wetting between the garnet solid-state electrolyte and molten lithium metal. Therefore, the reduction in the interfacial impedance is not optimum. Several methods have been studied to address the chemical stability and high interfacial impedance of the garnet oxides with the lithium metal, which are discussed further.

3.4.1. Surface polishing of the air-exposed oxides

It has been reported that oxide type garnets such as Ta-doped LLZO reacts with humid air forming an insulating Li_2CO_3 layer on its surface which decreases ionic conductivity[129]. Cheng et al. claimed that high interfacial impedance is due to the natural formation of Li_2CO_3 on the garnet solid-state electrolytes such as LLZO when exposed to air[130]. Surface polishing of the air exposed LLZO pellets was performed by using polishing papers with grit numbers ranging from 300 to 600, removing 50 μm thick layer from the surface. This approach led to the achievement of a very low interfacial area specific resistance of 109 Ωcm^2. Further, Li et al. attributed the large interfacial resistance in the garnet/Li interface to (1) blocking of Li$^+$ transfer at interface

due to Li^+/H^+ exchange at the garnet surface; (2) formation of insulating Li_2CO_3 layer on garnet surface; (3) Li-Al-O glassy phase on the garnet surface[131]. The group introduced carbon which reacts with Li_2CO_3 on the garnet surface when sintered at 700°C for 10 h, converting the garnet pellets from yellow into pure white. Interfacial resistance of 28 and 9 Ωcm^2 at 25°C and 65°C respectively were obtained for Li/LLZT-C/Li symmetric cells in comparison to Li/LLZT/Li cells with 1210 and 725 Ωcm^2 at 25 and 65°C, respectively.

### 3.4.2. Control on microstructure and grain boundary

Another method is to control the garnet's microstructure and grain boundary sizes. LLZO heterostructures with controlled compositions and microstructures were used to corelate the microstructures of solid ceramic LLZO electrolyte with interfacial resistances[132]. Interesting observation was done that showed a very low interfacial resistance of 37 Ωcm^2 and improved cycling performance for samples with small grains compared to large grain sizes.

3.4.3. Surface coatings

The surface of LLZO is lithiophobic, therefore conversion to a lithiophilic surface is essential to establish proper surface contact between LLZO and lithium metal. Lu et al. employed a simple approach of forming a stable SEI by immersing LLZTO-LZO surface in a molten Li-Al alloy[133]. An Al rich interface is spontaneously formed which helped to achieve a low interfacial resistance of less than 1 Ω cm^2. Symmetrical cell tests revealed a stable cycling up to 3000 h with high critical current density of 2.3 $mAcm^{-2}$ at 60 °C. Lu and coworkers employed an ultrathin amorphous Si coating on LLZO ($Li_{6.85}La_{2.9}Ca_{0.1}Zr_{1.75}Nb_{0.25}O_{12}$) garnet solid electrolyte using plasma enhanced chemical vapor deposition[134]. The Si coating converted the superlithiophobic LLZO surface into superlithiophilic, attributed to formation of lithiated Si formed by reaction between Li and Si. This was reflected on to the interfacial resistance between Li and LLZO, which reduced from 925 to 127 Ωcm^2 when compared to the uncoated LLZO. Similarly, the group deposited a thin germanium (Ge) layer on LLZO garnet by electron beam evaporation which forms a Li-Ge alloy upon contact with the lithium metal[135]. Similar reduction in interfacial resistance was observed with Ge-modified garnet showing 115 Ωcm^2 vs 900 Ωcm^2 for the uncoated LLZO. Full cell employing Ge-modified garnet coupled with $LiFePO_4$ cathode and Li metal demonstrated comparable cycling performance at room temperature to liquid electrolyte.

An ultrathin coating of aluminium oxide (Al_2O_3) was deposited on garnet $Li_7La_{2.75}Ca_{025}Zr_{1.75}Nb_{0.25}O_{12}$ (LLCZN) by atomic layer deposition (ALD) (Fig. 18a)[136]. The Al_2O_3 coating led to (1) improved wetting of the metallic lithium and LLCZN (Fig. 18b), and (2) the lithiated-Al_2O_3 interface provided an effective lithium ion transport between the lithium metal anode and the LLCZN. This approach led to a significant reduction in the interfacial impedance from 1,710 Ωcm^2 to 1 Ωcm^2 at room temperature (Fig. 18c). The Li/LLCZN/Li symmetrical cell with the ALD coating displayed a stable lithium plating and stripping with stabilized voltage at ~ 13 mV, while the cell without the ALD coating exhibited noisy voltage profile with large polarization. The Li/ALD-treated garnet/$Li_2FeMn_3O_8$ full cell showed a charge capacity of 110 $mAhg^{-1}$ over 50 cycles (Fig. 18d). Another similar approach was introduced by

forming an ultrathin, artificial intermediary Li-metal alloy. This was done by use of thin layer of Al to form an ionically conducting Li-Al alloy as the interfacial layer between the garnet solid-state electrolyte and the lithium metal [126]. This alloy improved the wettability of the garnet surface making it more lithiophilic and was able to decrease the interfacial resistance from 950 Ω cm^2 to 75 Ωcm^2. However, a hybrid solid-liquid Li-ion cell was demonstrated using LiFePO$_4$ cathode and the coated garnet which delivered initial charge/discharge capacities of 152 and 132 mAhg^{-1} and a good rate capability. Li-S and Li-O$_2$ cells with the hybrid solid-liquid electrolyte were also studied with the coated garnet.
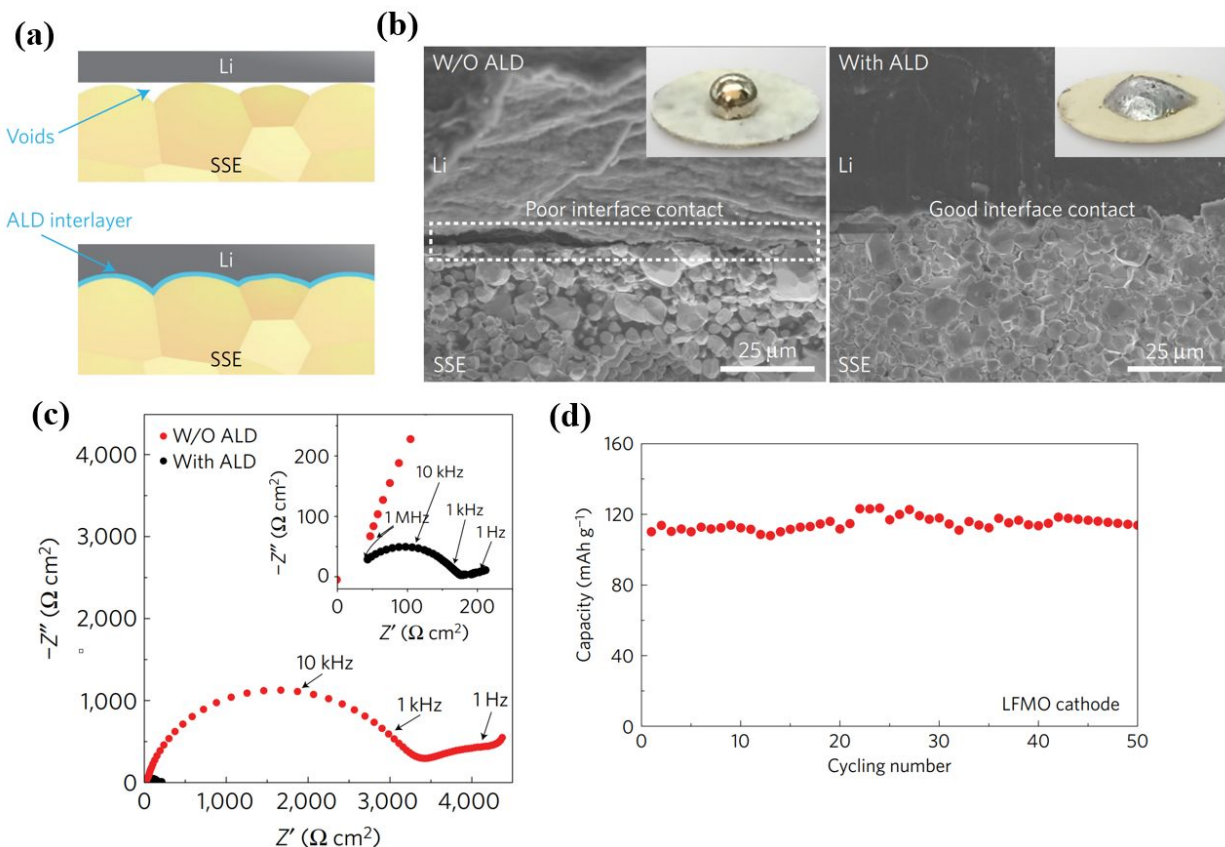
Fig. 18 Ultrathin coating of Al$_2$O$_3$ on Li$_7$La$_{2.75}$Ca$_{025}$Zr$_{1.75}$Nb$_{0.25}$O$_{12}$ garnet solid electrolyte. (a) Schematic showing the wettability of the garnet with molten Li; (b) Cross-sectional SEM images of the interface of garnet with Li metal, without and with the ALD deposited Al$_2$O$_3$; (c) Nyquist plots of Li/LLCZN/Li cells with and without ALD-Al$_2$O$_3$ coating on garnet, (Inset shows the magnified view of the impedance curve of the cell with ALD coating); (d) Cycling performance of the LFMO/ALD-garnet solid state electrolyte /Li full cell. Reproduced with permission from Ref [136]. Copyright (2016) Springer Nature.

Further, Fu et al. deposited metal film magnesium (Mg) on LLCZN garnet by sputtering[137]. Mg was found to diffuse into the bulk Li metal and form a Li-Mg alloy dominant interface between the garnet and Li metal. The transient dissolution behavior of this metal layer helped to realize intimate contact of the garnet with Li metal. Interfacial resistance for Li symmetric cell with Mg coating was 70 Ωcm^{-2}, which was minimal compared to cell without coating with 1000

Ωcm^{-2}. The symmetric cell showed stable cycling at current of 0.1 mAcm^{-2} during Li stripping/ plating test. An interesting observation was made that the interfacial resistance did not increase with increase in the metal layer thickness and was attributed to the transient behavior of the metal layer. Wang and coworkers deposited an ultrathin and conformal coating of ZnO on to LLCZN ($Li_{6.75}La_{2.75}Ca_{0.25}Zr_{1.75}Nb_{0.25}O_{12}$) by atomic layer deposition. ZnO facilitates reaction with Li metal and improves the wetting of the garnet with lithium metal [138]. This helped to achieve a low interfacial resistance of 20 $\Omega \cdot cm^2$ under 300 ˚C. Additionally, Shao et al. employed graphite as the interface modifier on top of the tungsten (W)-doped garnet $Li_{5.9}Al_{0.2}La_3Zr_{1.75}W_{0.25}O_{12}$ (LALZWO) garnet[139]. A very simple approach of drawing the graphite layer with a pencil on the garnet was adopted (Fig. 19a). This graphite-based soft interface forms lithiated graphite LiC_6, provides both ionic as well as electronic conductivity and improves the wettability of the molten lithium on to the garnet surface (Fig. 19b). This phenomenon led to achievement of decrease in interfacial impedance from 1350 to 105 $\Omega \cdot cm^2$ which indicated enhancement of interfacial contact between the garnet and Li metal (Fig. 19c). Symmetrical cells based on graphite modified garnet showed better cycling performance compared to the bare garnet (Fig. 19d). Further, a full cell consisting of Li metal anode, ternary NCM523 cathode and graphite modified garnet achieved excellent cell performance (Fig. 19e,f).
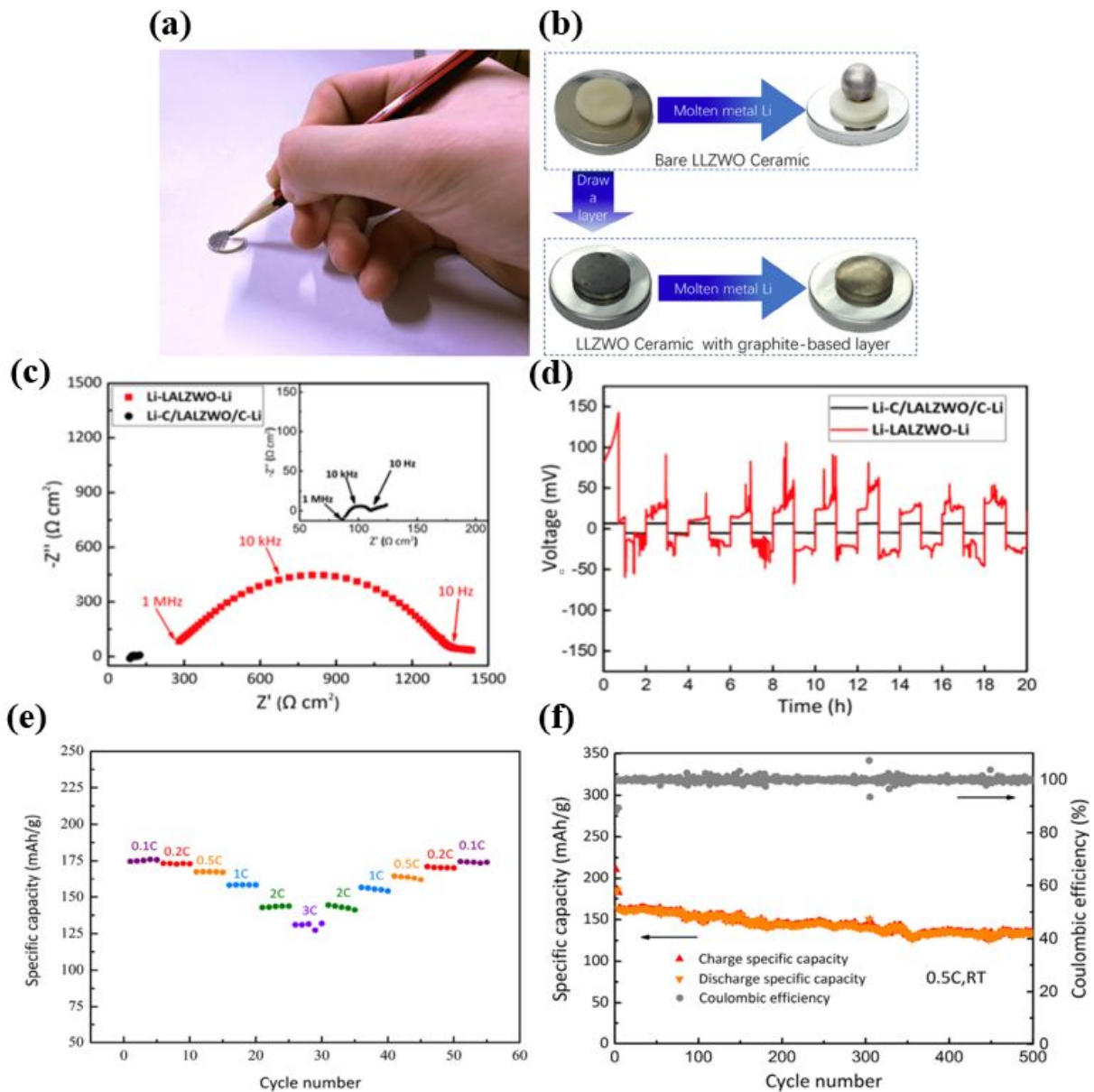
Fig. 19 Graphite-based soft interface modifier for LALZWO ceramic. (a) Schematic showing preparing graphite-based interface on the ceramic; (b) Wettability of molten lithium on the ceramic without and with the graphite-interface; (c) Nyquist plots and (d) voltage profiles at current density of 50 μAcm^{-2} of the Li/LALZWO/Li symmetrical cells without and with the graphite modified interface; (e) Rate capability and (f) Cycling performance of the all-solid-state full cell based on NCM523 cathode/graphite modified LALZWO/Li at 0.5 C at room temperature. Reproduced with permission from Ref [139]. Copyright (2018) American Chemical Society.

Xu et al. coated Li$_3$N on the surface of garnet using plasma enhanced chemical vapor deposition (PECVD)[140]. Li$_3$N was used because it has high Li$^+$ ion conductivity (10^{-3} Scm^{-1} at room temperature), improves wettability and interfacial contact between garnet electrolyte and

Li metal, suppresses Li dendrite growth as it protects reduction of the garnet electrolyte by Li metal. In this process, the Li_2CO_3 originally formed on the garnet surface was first removed by annealing with carbon, followed by the deposition of the thin Li_3N layer. Li symmetrical cells exhibited decrease of total interfacial impedance from 2512 Ωcm^2 for LC-LLZT to 180 Ωcm^2 for LN-LLZT at 60ºC and similarly 4785 Ωcm^2 to 350 Ωcm^2 at room temperature.

Although known solid polymer electrolytes shows low Li^+ ion conductivity at room temperature, their mechanical properties can be utilized for forming a thin, flexible and interface compatible SEI membrane that is easily wetted by lithium metal anode. Zhou et al. developed a polymer-ceramic single-ion-conducting solid electrolyte (PCSSE) by coating LLZTO pellet with a gel-solution of PEO-PAS using drop casting technique[141]. The decrease of interfacial impedance from 5000 Ω for Li/LLZTO/Li cell to 400 Ω for Li/PEO-PAS/LLZTO/PEO-PAS/Li cell. An all-solid-state Li/ PEO-PAS/LLZTO/PEO-PAS/LiFePO$_4$ cell exhibited capacity around 145 mAhg^{-1} at 0.1C and 140mAhg^{-1} at 0.2C.

Although most interfacial engineering approaches focus on introducing some ion conductive interfacial layers such as metal/metal oxide (Au, Si, Al, or Al_2O_3) or dry polymer, they need high temperature processing for manufacturing which is costly. Interlayer composed of gel electrolyte can be a cheaper alternative for scalable manufacturing. Liu et al. used gel polymer electrolyte (liquid electrolyte stored in PVDF-HFP polymer matrix)[142]. For this hybrid electrolyte design, interfacial resistance for garnet/Li interface decreased from 1.4×10^3 to 214 Ωcm^2. A full cell using LiFePO$_4$ as cathode demonstrated high capacity of 140mAhg^{-1} and was stable over 70 cycles at room temperature.

3.4.4. Introduction of additives

Garnet type material has better compatibility with Li metal and has high Li-ion conductivity. However, the garnet type electrolyte cannot suppress the dendrite formation, and thus short circuit can occur even at low current density. This has been attributed to the dendrite growth through the grain boundaries and voids in the electrolyte. To eliminate this phenomenon, Xu et.al and co-workers used Li_3PO_4 as an additive to LLZTO (Fig. 20a) [143]. This addition of Li_3PO_4 improved Li-ion conductivity of the garnet to 1.4×10^{-4} Scm^{-1} (Fig. 20b), improved interfacial resistance with lower resistance (Fig. 20c) and suppressed Li-dendrite formation during the plating and stripping of lithium with stable cycling (Fig. 20d).

Wang et al. prepared an assistant ionic conductor by infusing an ionic liquid (Li-IL) into porous metal-organic framework (MOF) host[144]. The pristine LLZO showed ionic conductivity of 1.5×10^{-6} S cm^{-1} at 30 ºC, which increased to 4.1×10^{-5}, 7.1×10^{-5}, 1.0×10^{-4}, and 1.3×10^{-4} Scm^{-1} as 5 wt%, 10 wt%, 20 wt%, and 30 wt% LIM (LiTFSI dissolved in [EMIM][TFSI]) was added, respectively. The introduction of ionic liquid impregnated MOF into LLZO SSE can improve the conductivity as well as effectively decrease the interfacial resistance due to formation of nanowetted interface between electrolyte and Li metal. Composites of glassy amorphous Li-ion conductors and ceramic based garnets can enhance its wettability and have good chemical stability with Li metal in electrolyte/Li interface. Tian et al. prepared a composite of LLZTO garnet and amorphous Li_3OCl antiperovskite Li-ion conducting materials[145]. Only 2 wt % of

Li$_3$OCl was added that acted as binder, filler and bridge in LLZTO network to promote the ionic conductivity (2.27x10^{-4} Scm^{-1}) and enhance the interfacial contact at room temperature. Formation of dense and stable interfacial layer as a result of reaction between Li metal and Li$_3$OCl increases the wettability of lithium anode to solid electrolyte and hence, the interfacial resistance decreased from 1850 to 90 Ωcm^2. Also, an all-solid-state LiFePO$_4$/LLZTO-2wt% Li$_3$OCL/Li battery exhibited specific capacity of 157.5 mAhg^{-1} and 85.7 mAhg^{-1} at 0.05C and 0.5C, respectively.
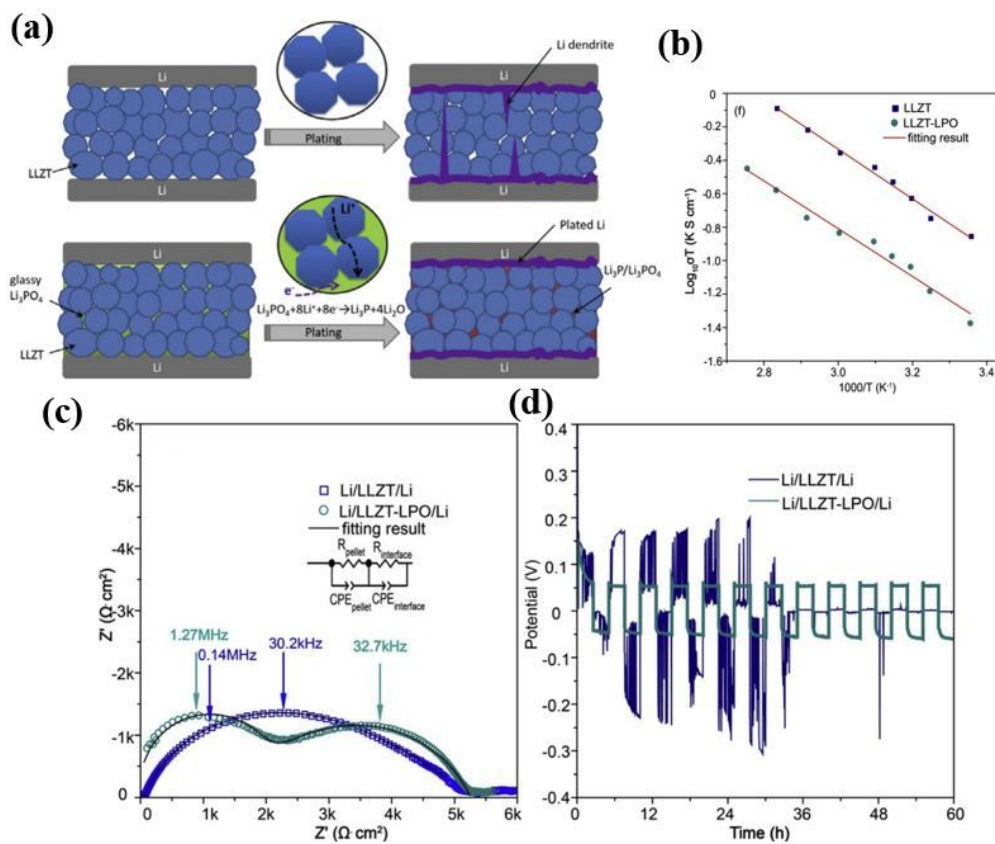
Fig. 20 Li$_3$PO$_4$-modified LLZTO garnet. (a) Schematic showing the suppression of lithium dendrites by addition of Li$_3$PO$_4$ into the garnet; (b) Arrhenius plots of the garnet without and with Li$_3$PO$_4$; (c) Nyquist plots and (d) voltage profiles of symmetrical cells Li/Garnet/Li without and with Li$_3$PO$_4$. Reproduced with permission from Ref [143].Copyright (2017) Elsevier.

3.4.5. 3D conductive framework

Most of the solid polymer electrolytes are flexible in nature, consequently this property can help to fill up the voids that exist between Li metal and garnet interface. Chi et al. employed a solid polymer electrolyte based on PEO-LiTFSI in acetonitrile to modify the surface of the LLZTO garnet[146]. In addition to this, a 3D lithium metal prepared by molten lithium infusion in Ni foam was used. This combination of the interface modification by solid polymer electrolyte and use of 3D lithium led to superior symmetrical cell performance compared to the non-modified

interface and bare Li electrode. Further, full cell consisting of LFP/SPE-LLZTO-SPE/3D Li exhibited excellent cyclability at 0.2 C and 90˚C.

Yang et al. demonstrated hosting Li metal in a 3D garnet-type ion conductive framework with a planar current collector at the bottom[147]. This structure enables Li plating from the bottom Cu current collector and rising during deposition. This approach facilitates lithium rise/fall away from the separator which would prevent internal short circuits due to lithium penetration. Meanwhile, the porous structure mitigates the volume change of the Li anode. A stable cycling up to 300 h at 0.5 mAcm^{-2}, 1 mAhcm^{-2} was demonstrated with the lithium metal in the garnet host. Liu et al. adopted 3D Li and a flowable interfacial layer to address the interfacial fluctuation that exists for the Li anode (Fig. 21a,b) [148]. A 3D rGO electrode filled with molten lithium was used as the 3D Li anode with high electroactive surface area, while a PEG plasticized with LiTFSI was impregnated into the 3D Li by thermal infiltration at 150 ˚C to form the flowable interfacial layer. The 3D Li along with the flowable interfacial layer helps to accommodate the interfacial fluctuation, thus maintaining the intimate contact. The modified Li when used in a full cell with a LLZTO garnet along with LFP, exhibited much lower charge/discharge overpotential as well as superior rate capability compared to the conventional Li foil (Fig. 21c,d). Fu et al. prepared a 3D bilayer garnet solid-state electrolyte framework that consists of thick porous layer and thin dense layer using tape casting process (Fig. 22a,b) [149]. The thick porous layer provides mechanical support and further serves as host that enables high loading of cathode materials. While, the dense layer acts as blocking element of physical and chemical short circuits that can occur due to volume changes and dendrite formation during charge/discharge cycles between the active electrodes. For electrochemical characterization of garnet/Li metal interface, a polymeric gel layer was coated on the garnet surface (Fig. 22c). Sulfur was directly coated into porous garnet layer by melting sulfur powder into the porous matrix, enabling higher sulfur mass loading of around 7.5 mgcm^{-2}. A hybrid Li-S cell exhibited discharge capacity around 645 mAhg^{-1} for the 1st cycle and coulombic efficiency of 99.8% with good cycling performance (Fig. 22d,e).
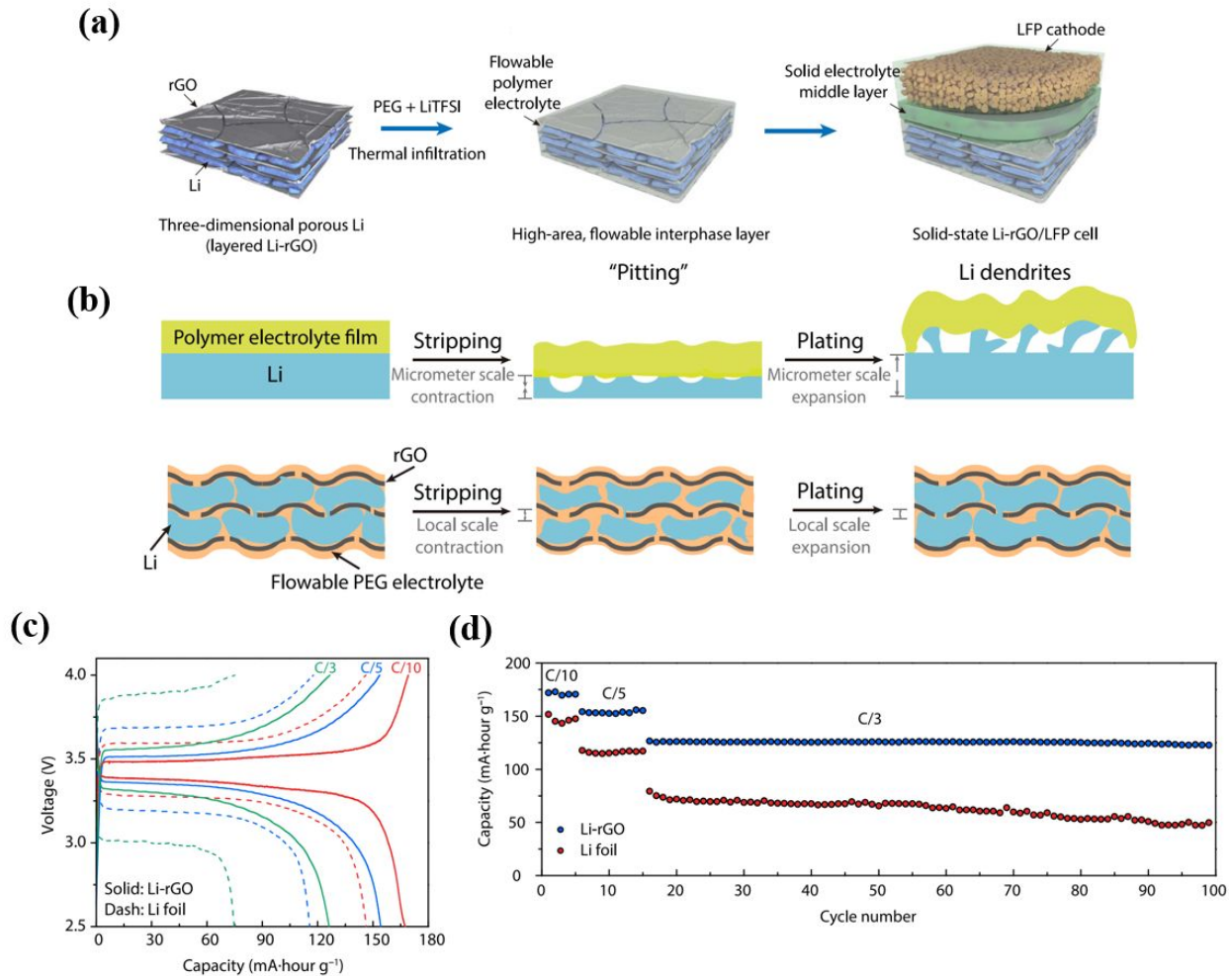
Fig. 21 3D Li anode with flowable interphase. (a) Schematic showing fabrication of 3D Li-rGO composite via thermal infiltration of PEG-LiTFSI at 150 °C and construction of an all-solid-state Li-LFP full cell; (b) Schematics showing comparison of Li stripping/plating between conventional Li foil anode and the 3D-rGO anode as lithium host; Solid-state Li-LFP full cell with LLZTO as middle layer and either 3D Li-rGO or Li foil as anode (c) Charge/discharge voltage curves and (d) cycling performance. Reproduced with permission from Ref [148]. Copyright (2017) American Association for the Advancement of Science.
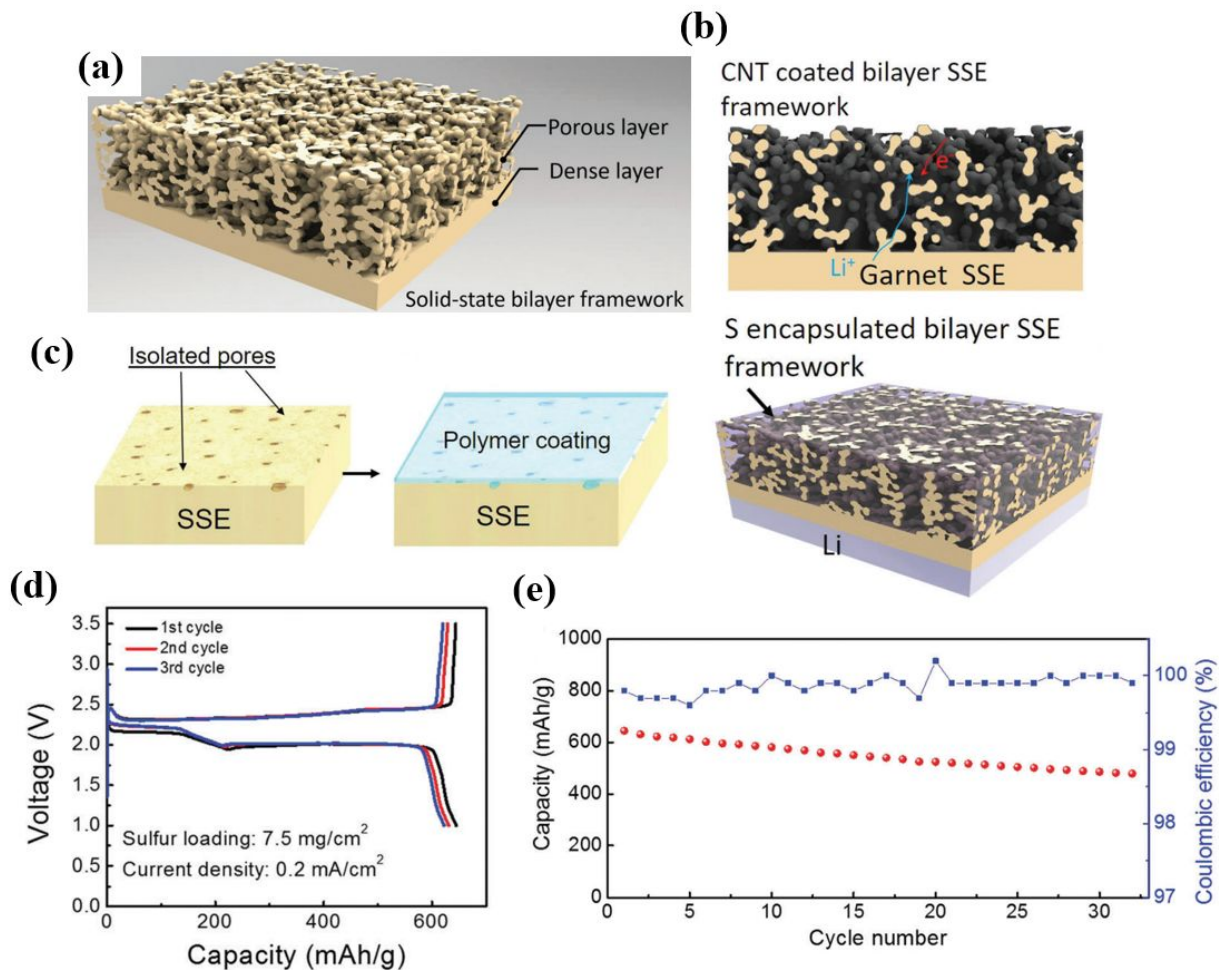
Fig. 22 3D bilayer garnet solid electrolyte. (a) Schematic of the garnet bilayer framework; (b) Schematic of the CNT coated and S-encapsulated garnet based all solid-state Li-S battery; (d) Charge/discharge voltage profiles and (e) Cycling performance of the solid-state Li-S battery. Reproduced with permission from Ref [149]. Copyright (2017) Royal Society of Chemistry.

Among different types of solid electrolyte, composite polymer electrolytes show acceptable Li-ion conductivity. However, in these types of composites, high concentration of nanofillers degrades the performance of battery due to agglomeration of these nanofillers in polymeric chain that destroys the percolated network of interphase. This inhibits the improvement in Li-ion conductivity for these composite polymer electrolytes. To overcome this, Bae et al. designed a 3D nanofiller, nanostructured hydrogel-derived $Li_{0.35}La_{0.55}TiO_3$(LLTO) framework for fabrication of composite polymer Li-ion electrolyte[150]. The approach herein to fabricate a 3D nanostructured hydrogel derived pre-percolated LLTO was for avoiding particle agglomeration while mixing with polymer electrolyte. Avoiding particle agglomeration using interconnected 3D percolating nanostructure yields numerous continuous Li-ion conduction pathways. The Li-ion conductivity of about 10^{-4} Scm^{-1} was observed at room temperature of these composite solid electrolytes. Li and coworkers demonstrated a 3D fiber-network reinforced bicontinuous solid composite electrolyte by electrospinning precursor of

lithium aluminum phosphate (LATP)/ polyacrylonitrile (PAN) mixed in DMF and casting PEO and LiTFSI mixture onto it[151]. Thus, obtained composite electrolyte had high stability against Li metal and good interfacial contact with Li anode. The ionic conductivity of xLATP/PAN-[PEO$_8$-LiTFSI], where x=2 (x: mass ratios of LATP to PAN) was about 6.5×10^{-4} Scm^{-1} which is four times higher than that of PEO$_8$-LiTFSI control electrolyte. The interfacial resistance for symmetric Li| 2LATP/PAN-[PEO$_8$-LiTFSI] |Li cell was 158 Ω at 60°C which is much lower in comparison to Li|LATP|Li cell (>3500Ω at 60°C). This decrease in resistance and increase in interface wettability with Li metal can be attributed to increased interface contact area between the composite electrolyte nanofibers and Li electrode.

4.   Conclusion, Opportunities and Outlook

Solid-state lithium batteries are believed to be the future and the energy storage industry is optimistic about it. Significant research and efforts are underway to bring this technology to the mass market. This has led to development of solid-state electrolytes with comparable ionic conductivity to conventional liquid electrolyte. While major focus has been on improvement of ionic conductivity of these solid electrolytes, it is equally important to consider their compatibility with electrodes in order to realize a working all-solid-state battery. This review summarized the notable efficient approaches that have addressed the interfacial issues of solid-state electrolyte systems (sulfides and oxides) with both battery cathode and lithium anode. Both the sulfide and oxides (garnets and NASICON) have their own unique electrochemical, thermal and mechanical features, therefore, the approaches that have been applied to address their interfacial incompatibility with battery electrodes are different from one another. With several significant advances already achieved, the likelihood of adoption of the solid-state technology even for large scale energy applications such as electric vehicles and grids is high, considering the cost.

Majority of the research reports are dedicated to address either the lithium/SSE or the cathode/SSE interface. However, a practical solid-state LMB should have both these interfaces equally efficient and stable. Therefore, it is imperative to modify both the interfaces to construct a working solid-state full cell. However, each electrolyte system has its own interfacial imperfections, therefore, there is no solution in the form of a single strategy that will be constructive to every electrolyte system. Consequently, it is key to treat each electrolyte system and their interfaces independently. It should be noted that interfacial processes in solid-state LMBs are complicated in nature and therefore, thorough dedicated research is imperative. Multiple interfacial issues need to be addressed when considering the fabrication of the solid-state LMB which can be summarized into two primary factors: (i) chemical and electrochemical compatibility and (ii) intimate mechanical contact. Interfacial surface chemistry is a complicated phenomenon that determines the formation of interphase layers and their electronic and ionic conductivity properties. It is a very challenging to find an electrolyte that exhibits excellent chemical/electrochemical compatibility and mechanical stability with both lithium anode and cathode. Therefore, research in finding such electrolyte should be focused as both the interfaces

(with lithium and cathode) play equally crucial roles. For this, computational studies on novel materials should be prioritized.

Based on the above review of the individual interfaces, we believe that these three directions should be adopted to build an interface compatible solid-state LMB namely (i) hybrid ceramic/polymer composite electrolyte, (ii) surface coating and (iii) 3D scaffolds infusing Li. Use of hybrid electrolyte can be advantageous for both cathode/SSE and Li/SSE interfaces and should be adopted. Each electrolyte system (either oxides or sulfides) has its own advantages but some shortcomings. Synergistic combination of the properties of ceramics to that of polymer electrolyte systems can help to overcome each other's intrinsic limitations. Solid polymer electrolytes have much better flexibility and adhesion properties with electrodes. This suggests that the addition of polymers can assist on the processability of the ceramics and help achieve intimate mechanical contact especially with the cathodes. In addition, polymers can facilitate the necessary buffering function to relieve stress/strain caused upon volume change of the electrodes. Further, the Li-ion conducting polymers can exhibit good electrochemical stability with Li at the interface, thus contributing to low voltage polarization. These composite electrolytes basically combine the constructive properties of the two electrolyte systems, and some studies have shown positive outcomes[152-154]. Further, the inorganic solid-state electrolytes have also been employed as additives or fillers into the polymer matrix and demonstrated to have a positive effect on the ionic conductivity and electrochemical performance of the polymer solid electrolytes[155, 156]. On the other hand, a conformal surface coating of suitable *in situ* or *ex situ* interphase layer on Li metal and cathode coating to form cathode/electrolyte composite have been the most effective approaches to address the interface incompatibility, which we believe the battery research should further advance at much greater extent. Further, the 3D scaffolds (e.g. rGO, metal foams) with Li infusion technique that have the capability of accommodating the interfacial fluctuation during cycling should be adopted, which has been rigorously studied for lithium dendrite suppression for liquid electrolyte-based lithium metal battery systems[157-160]. In addition, numerous efforts have been carried out on interface modifications with lithium metal for a liquid electrolyte system[17]. Findings and understanding obtained from these investigations can be directly experimented in solid-state electrolyte systems. However, it is most likely that a single technique alone will not be able to solve the impedance problem entirely. Therefore, implementing a combination of these approaches should be considered to realize a practical bulk solid-state LMB.

Detailed information on the interface products formed at the interfaces is still unknown, which will be unique for each electrolyte and interface systems. *In situ* or operando and other advanced characterization techniques are being currently pursued to gather real time information and analysis during lithiation and delithiation process such as *in situ* XPS, *in situ* TEM, *in situ* NMR, *in situ* XRD, cryo-TEM. The use of these advanced techniques should be heavily encouraged to obtain insights of these complex interface issues existing in solid-state lithium batteries. Further, fundamental understanding of the factors and mechanisms contributing to these interface issues should be prioritized. A recent study investigated the process of lithium dendrite growth and infiltration in inorganic solid electrolytes. The study showed that the lithium penetration is dependent on defect size and density rather than the impact of electrolyte shear modulus and surface roughness, and that faster Li dendrite growth is dominated by cracks, grain

boundaries and/or micro/nanoscale pores[161]. Further, a study on origin of dendrite formation in LLZO and Li_3PS_4 representative solid electrolytes during lithium plating was carried out using time-resolved operando neutron depth profiling, which suggested that the high electronic conductivity of these solid electrolytes is responsible for the dendrite formation[162]. Such fundamental findings will be key to better understand the solid-solid interfaces and contribute to building efficient and safe all-solid-state batteries. In addition, theoretical modeling based on machine learning should be employed for high-throughput materials screening to develop efficient and stable interfaces.

Scalability of the technology should also be taken into consideration with low-cost manufacturability. The methodology and the fabrication involved should line up with the current lithium-ion production infrastructure to enable a transferable technology into industry. This can facilitate mass production without imposing substantial financial burden.

Conflicts of Interest
There are no conflicts to declare.

References

1. Z. Yang, J. Zhang, M. C. Kintner-Meyer, X. Lu, D. Choi, J. P. Lemmon and J. Liu, *Chemical reviews*, 2011, **111**, 3577-3613.
2. A. Gurung and Q. Qiao, *Joule*, 2018, **2**, 1217-1230.
3. J. B. Goodenough and K.-S. Park, *Journal of the American Chemical Society*, 2013, **135**, 1167-1176.
4. J. M. Tarascon and M. Armand, *Nature*, 2001, **414**, 359-367.
5. M. Armand and J.-M. Tarascon, *nature*, 2008, **451**, 652.
6. S. Liu, W. Lei, Y. Liu, Q. Qiao and W.-H. Zhang, *ACS applied materials & interfaces*, 2018, **10**, 37445-37452.
7. R. Naderi, A. Gurung, Z. Zhou, G. Varnekar, K. Chen, J. Zai, X. Qian and Q. Qiao, *Advanced Sustainable Systems*, 2017, **1**, 1700043.
8. S. J. Varapragasam, C. Balasanthiran, A. Gurung, Q. Qiao, R. M. Rioux and J. D. Hoefelmeyer, *The Journal of Physical Chemistry C*, 2017, **121**, 11089-11099.
9. Z. Zhou, H. Zhang, Y. Zhou, H. Qiao, A. Gurung, R. Naderi, H. Elbohy, A. L. Smirnova, H. Lu and S. Chen, *Scientific reports*, 2017, **7**, 1440.
10. H. Qiao, Z. Xia, Y. Liu, R. Cui, Y. Fei, Y. Cai, Q. Wei, Q. Yao and Q. Qiao, *Applied Surface Science*, 2017, **400**, 492-497.
11. A. Gurung, R. Naderi, B. Vaagensmith, G. Varnekar, Z. Zhou, H. Elbohy and Q. Qiao, *Electrochimica Acta*, 2016, **211**, 720-725.

12.   M. Dondelinger, J. Swanson, G. Nasymov, C. Jahnke, Q. Qiao, J. Wu, C. Widener, A. M. Numan-Al-Mobin and A. Smirnova, *Electrochimica Acta*, 2019, **306**, 498-505.

13.   M. McGraw, P. Kolla, B. Yao, R. Cook, Q. Quiao, J. Wu and A. Smirnova, *Polymer*, 2016, **99**, 488-495.

14.   Y. Liu, Y. Zhu and Y. Cui, *Nature Energy*, 2019, 1.

15.   R. Pathak, A. Gurung, H. Elbohy, K. Chen, K. M. Reza, B. Bahrami, S. Mabrouk, R. Ghimire, M. Hummel, Z. Gu, X. Wang, Y. Wu, Y. Zhou and Q. Qiao, *Nanoscale*, 2018, **10**, 15956-15966.

16.   Y. Sun, L. Wang, Y. Li, Y. Li, H. R. Lee, A. Pei, X. He and Y. Cui, *Joule*, 2019, **3**, 1080-1093.

17.   D. Lin, Y. Liu and Y. Cui, *Nature Nanotechnology*, 2017, **12**, 194.

18.   Y. Sun, N. Liu and Y. Cui, *Nature Energy*, 2016, **1**, 16071.

19.   H. Wu and Y. Cui, *Nano Today*, 2012, **7**, 414-429.

20.   A. Gurung, R. Naderi, B. Vaagensmith, G. Varnekar, Z. Zhou, H. Elbohy and Q. Qiao, *Electrochimica Acta*, 2016, **211**, 720-725.

21.   W.-J. Zhang, *Journal of Power Sources*, 2011, **196**, 13-24.

22.   C. K. Chan, H. Peng, G. Liu, K. McIlwrath, X. F. Zhang, R. A. Huggins and Y. Cui, *Nature Nanotechnology*, 2007, **3**, 31.

23.   X. Su, Q. Wu, J. Li, X. Xiao, A. Lott, W. Lu, B. W. Sheldon and J. Wu, *Advanced Energy Materials*, 2014, **4**, 1300882.

24.   P. Li, G. Zhao, X. Zheng, X. Xu, C. Yao, W. Sun and S. X. Dou, *Energy Storage Materials*, 2018, **15**, 422-446.

25.   X. Shen, Z. Tian, R. Fan, L. Shao, D. Zhang, G. Cao, L. Kou and Y. Bai, *Journal of Energy Chemistry*, 2018, **27**, 1067-1090.

26.   M. Zhang, T. Zhang, Y. Ma and Y. Chen, *Energy Storage Materials*, 2016, **4**, 1-14.

27.   X. Zuo, J. Zhu, P. Müller-Buschbaum and Y.-J. Cheng, *Nano Energy*, 2017, **31**, 113-143.

28.   W. Xu, J. Wang, F. Ding, X. Chen, E. Nasybulin, Y. Zhang and J.-G. Zhang, *Energy & Environmental Science*, 2014, **7**, 513-537.

29.   H. Kim, G. Jeong, Y.-U. Kim, J.-H. Kim, C.-M. Park and H.-J. Sohn, *Chemical Society Reviews*, 2013, **42**, 9011-9034.

30.   X.-B. Cheng, R. Zhang, C.-Z. Zhao and Q. Zhang, *Chemical Reviews*, 2017, **117**, 10403-10473.

31.   S. Li, M. Jiang, Y. Xie, H. Xu, J. Jia and J. Li, *Advanced Materials*, 2018, **30**, 1706375.

32.   H. Yang, C. Guo, A. Naveed, J. Lei, J. Yang, Y. Nuli and J. Wang, *Energy Storage Materials*, 2018, **14**, 199-221.

33.   J. Lang, L. Qi, Y. Luo and H. Wu, *Energy Storage Materials*, 2017, **7**, 115-129.

34.   K. Chen, R. Pathak, A. Gurung, E. A. Adhamash, B. Bahrami, Q. He, H. Qiao, A. L. Smirnova, J. J. Wu, Q. Qiao and Y. Zhou, *Energy Storage Materials*, 2019, **18**, 389-396.

35.   P. G. Bruce, S. A. Freunberger, L. J. Hardwick and J.-M. Tarascon, *Nature Materials*, 2011, **11**, 19.

36.   Z. W. Seh, Y. Sun, Q. Zhang and Y. Cui, *Chemical Society Reviews*, 2016, **45**, 5605-5634.

37.   D. Aurbach, B. D. McCloskey, L. F. Nazar and P. G. Bruce, *Nature Energy*, 2016, **1**, 16128.

38.   Q. Pang, X. Liang, C. Y. Kwok and L. F. Nazar, *Nature Energy*, 2016, **1**, 16132.

39.   J. Lu, L. Li, J.-B. Park, Y.-K. Sun, F. Wu and K. Amine, *Chemical Reviews*, 2014, **114**, 5611-5640.

40.   L. Grande, E. Paillard, J. Hassoun, J.-B. Park, Y.-J. Lee, Y.-K. Sun, S. Passerini and B. Scrosati, *Advanced Materials*, 2015, **27**, 784-800.

41.   E. Quartarone and P. Mustarelli, *Chemical Society Reviews*, 2011, **40**, 2525-2540.

42.   D. Aurbach, E. Zinigrad, Y. Cohen and H. Teller, *Solid state ionics*, 2002, **148**, 405-416.

43.   J. C. Bachman, S. Muy, A. Grimaud, H.-H. Chang, N. Pour, S. F. Lux, O. Paschos, F. Maglia, S. Lupart, P. Lamp, L. Giordano and Y. Shao-Horn, *Chemical Reviews*, 2016, **116**, 140-162.

44.   A. Manthiram, X. Yu and S. Wang, *Nature Reviews Materials*, 2017, **2**, 16103.

45.   J. Li, C. Ma, M. Chi, C. Liang and N. J. Dudney, *Advanced Energy Materials*, 2015, **5**, 1401408.

46.   L. Fan, S. Wei, S. Li, Q. Li and Y. Lu, *Advanced Energy Materials*, 2018, **8**, 1702657.

47.   Z. Xue, D. He and X. Xie, *Journal of Materials Chemistry A*, 2015, **3**, 19218-19253.

48.   S. Chen, D. Xie, G. Liu, J. P. Mwizerwa, Q. Zhang, Y. Zhao, X. Xu and X. Yao, *Energy Storage Materials*, 2018, **14**, 58-74.

49.   N. Kamaya, K. Homma, Y. Yamakawa, M. Hirayama, R. Kanno, M. Yonemura, T. Kamiyama, Y. Kato, S. Hama, K. Kawamoto and A. Mitsui, *Nature Materials*, 2011, **10**, 682.

50.   Y. Kato, S. Hori, T. Saito, K. Suzuki, M. Hirayama, A. Mitsui, M. Yonemura, H. Iba and R. Kanno, *Nature Energy*, 2016, **1**, 16030.

51.   A. Junji, T. Akira, K. Kunimitsu, K. Norihito, I. Yasushi and A. Junji, *Chemistry Letters*, 2011, **40**, 60-62.

52.   K. Kerman, A. Luntz, V. Viswanathan, Y.-M. Chiang and Z. Chen, *Journal of The Electrochemical Society*, 2017, **164**, A1731-A1744.

53.   V. Thangadurai, H. Kaack and W. J. F. Weppner, *Journal of the American Ceramic Society*, 2003, **86**, 437-440.

54.   H. Buschmann, J. Dölle, S. Berendts, A. Kuhn, P. Bottke, M. Wilkening, P. Heitjans, A. Senyshyn, H. Ehrenberg, A. Lotnyk, V. Duppel, L. Kienle and J. Janek, *Physical Chemistry Chemical Physics*, 2011, **13**, 19378-19392.

55.   R. Murugan, V. Thangadurai and W. Weppner, *Angewandte Chemie International Edition*, 2007, **46**, 7778-7781.

56.   X. B. Cheng, R. Zhang, C. Z. Zhao, F. Wei, J. G. Zhang and Q. Zhang, *Advanced Science*, 2016, **3**, 1500213.

57.   S. Wenzel, S. Randau, T. Leichtweiß, D. A. Weber, J. Sann, W. G. Zeier and J. r. Janek, *Chemistry of Materials*, 2016, **28**, 2400-2407.

58.   S. Wenzel, T. Leichtweiss, D. Krüger, J. Sann and J. Janek, *Solid State Ionics*, 2015, **278**, 98-105.

59.   A. Sakuda, A. Hayashi and M. Tatsumisago, *Chemistry of Materials*, 2009, **22**, 949-956.

60.   J. Haruyama, K. Sodeyama and Y. Tateyama, *ACS Applied Materials & Interfaces*, 2017, **9**, 286-292.

61.   N. Ohta, K. Takada, L. Zhang, R. Ma, M. Osada and T. Sasaki, *Advanced Materials*, 2006, **18**, 2226-2229.

62.   Y. Seino, T. Ota and K. Takada, *Journal of Power Sources*, 2011, **196**, 6488-6492.

63.   N. Ohta, K. Takada, I. Sakaguchi, L. Zhang, R. Ma, K. Fukuda, M. Osada and T. Sasaki, *Electrochemistry Communications*, 2007, **9**, 1486-1490.

64.   K. Takada, N. Ohta, L. Zhang, X. Xu, B. T. Hang, T. Ohnishi, M. Osada and T. Sasaki, *Solid State Ionics*, 2012, **225**, 594-597.

65.   X. Xu, K. Takada, K. Fukuda, T. Ohnishi, K. Akatsuka, M. Osada, B. T. Hang, K. Kumagai, T. Sekiguchi and T. Sasaki, *Energy & Environmental Science*, 2011, **4**, 3509-3512.

66.   A. Sakuda, H. Kitaura, A. Hayashi, K. Tadanaga and M. Tatsumisago, *Electrochemical and Solid-State Letters*, 2008, **11**, A1-A3.

67.   A. Sakuda, H. Kitaura, A. Hayashi, K. Tadanaga and M. Tatsumisago, *Journal of Power Sources*, 2009, **189**, 527-530.

68.   A. Sakuda, N. Nakamoto, H. Kitaura, A. Hayashi, K. Tadanaga and M. Tatsumisago, *Journal of Materials Chemistry*, 2012, **22**, 15247-15254.

69.   A. Sakuda, H. Kitaura, A. Hayashi, M. Tatsumisago, Y. Hosoda, T. Nagakane and A. Sakamoto, *All-solid-state Lithium Secondary Batteries Using Li2S–P2S5 Solid Electrolytes and LiFePO4 Electrode Particles with Amorphous Surface Layer*, 2012.

70.   S. Ito, S. Fujiki, T. Yamada, Y. Aihara, Y. Park, T. Y. Kim, S.-W. Baek, J.-M. Lee, S. Doo and N. Machida, *Journal of Power Sources*, 2014, **248**, 943-950.

71.   N. Machida, J. Kashiwagi, M. Naito and T. Shigematsu, *Solid State Ionics*, 2012, **225**, 354-358.

72.   K. Okada, N. Machida, M. Naito, T. Shigematsu, S. Ito, S. Fujiki, M. Nakano and Y. Aihara, *Solid State Ionics*, 2014, **255**, 120-127.
73.   J. Kim, M. Kim, S. Noh, G. Lee and D. Shin, *Enhanced electrochemical performance of surface modified LiCoO2 for all-solid-state lithium batteries*, 2015.
74.   H. Kitaura, A. Hayashi, T. Ohtomo, S. Hama and M. Tatsumisago, *Journal of Materials Chemistry*, 2011, **21**, 118-124.
75.   D. H. Kim, D. Y. Oh, K. H. Park, Y. E. Choi, Y. J. Nam, H. A. Lee, S.-M. Lee and Y. S. Jung, *Nano Letters*, 2017, **17**, 3013-3020.
76.   A. Sakuda, A. Hayashi, T. Ohtomo, S. Hama and M. Tatsumisago, *Electrochemical and Solid-State Letters*, 2010, **13**, A73-A75.
77.   A. Sakuda, A. Hayashi, T. Ohtomo, S. Hama and M. Tatsumisago, *Journal of Power Sources*, 2011, **196**, 6735-6741.
78.   Y. Ito, M. Otoyama, A. Hayashi, T. Ohtomo and M. Tatsumisago, *Journal of Power Sources*, 2017, **360**, 328-335.
79.   K. Aso, A. Sakuda, A. Hayashi and M. Tatsumisago, *ACS Applied Materials & Interfaces*, 2013, **5**, 686-690.
80.   R. C. Xu, X. L. Wang, S. Z. Zhang, Y. Xia, X. H. Xia, J. B. Wu and J. P. Tu, *Journal of Power Sources*, 2018, **374**, 107-112.
81.   A. Hayashi, Y. Nishio, H. Kitaura and M. Tatsumisago, *Electrochemistry Communications*, 2008, **10**, 1860-1863.
82.   X. Yao, D. Liu, C. Wang, P. Long, G. Peng, Y.-S. Hu, H. Li, L. Chen and X. Xu, *Nano Letters*, 2016, **16**, 7148-7154.
83.   M. Nagao, A. Hayashi and M. Tatsumisago, *Electrochimica Acta*, 2011, **56**, 6055-6059.
84.   M. Nagao, A. Hayashi and M. Tatsumisago, *Journal of Materials Chemistry*, 2012, **22**, 10015-10020.
85.   M. Nagao, A. Hayashi, M. Tatsumisago, T. Ichinose, T. Ozaki, Y. Togawa and S. Mori, *Journal of Power Sources*, 2015, **274**, 471-476.
86.   F. Han, T. Gao, Y. Zhu, K. J. Gaskell and C. Wang, *Advanced Materials*, 2015, **27**, 3473-3483.
87.   S. Ohta, T. Kobayashi, J. Seki and T. Asaoka, *Journal of Power Sources*, 2012, **202**, 332-335.
88.   T. Matsuyama, R. Takano, K. Tadanaga, A. Hayashi and M. Tatsumisago, *Solid State Ionics*, 2016, **285**, 122-125.
89.   H.-S. Kim, Y. Oh, K. H. Kang, J. H. Kim, J. Kim and C. S. Yoon, *ACS applied materials & interfaces*, 2017, **9**, 16063-16070.
90.   K. Park, B.-C. Yu, J.-W. Jung, Y. Li, W. Zhou, H. Gao, S. Son and J. B. Goodenough, *Chemistry of Materials*, 2016, **28**, 8051-8059.
91.   L. Miara, A. Windmüller, C.-L. Tsai, W. D. Richards, Q. Ma, S. Uhlenbruck, O. Guillon and G. Ceder, *ACS applied materials & interfaces*, 2016, **8**, 26842-26850.
92.   B. Liu, K. Fu, Y. Gong, C. Yang, Y. Yao, Y. Wang, C. Wang, Y. Kuang, G. Pastel and H. Xie, *Nano letters*, 2017, **17**, 4917-4923.
93.   S. Ohta, S. Komagata, J. Seki, T. Saeki, S. Morishita and T. Asaoka, *Journal of Power Sources*, 2013, **238**, 53-56.
94.   F. Han, J. Yue, C. Chen, N. Zhao, X. Fan, Z. Ma, T. Gao, F. Wang, X. Guo and C. Wang, *Joule*, 2018, **2**, 497-508.
95.   T. Liu, Y. Ren, Y. Shen, S.-X. Zhao, Y. Lin and C.-W. Nan, *Journal of Power Sources*, 2016, **324**, 349-357.
96.   Z. Zhang, Y. Zhao, S. Chen, D. Xie, X. Yao, P. Cui and X. Xu, *Journal of Materials Chemistry A*, 2017, **5**, 16984-16993.
97.   W. Zha, Y. Xu, F. Chen, Q. Shen and L. Zhang, *Solid State Ionics*, 2019, **330**, 54-59.

98.   H. Duan, Y.-X. Yin, Y. Shi, P.-F. Wang, X.-D. Zhang, C.-P. Yang, J.-L. Shi, R. Wen, Y.-G. Guo and L.-J. Wan, *Journal of the American Chemical Society*, 2017, **140**, 82-85.

99.   T. Kato, T. Hamanaka, K. Yamamoto, T. Hirayama, F. Sagane, M. Motoyama and Y. Iriyama, *Journal of Power Sources*, 2014, **260**, 292-298.

100.   C. Wang, L. Zhang, H. Xie, G. Pastel, J. Dai, Y. Gong, B. Liu, E. D. Wachsman and L. Hu, *Nano energy*, 2018, **50**, 393-400.

101.   J. Van Den Broek, S. Afyon and J. L. Rupp, *Advanced Energy Materials*, 2016, **6**, 1600736.

102.   Z. Lu, J. Yu, J. Wu, M. B. Effat, S. C. Kwok, Y. Lyu, M. M. Yuen and F. Ciucci, *Energy Storage Materials*, 2019, **18**, 311-319.

103.   R. Xu, F. Han, X. Ji, X. Fan, J. Tu and C. Wang, *Nano Energy*, 2018, **53**, 958-966.

104.   A. Kato, A. Hayashi and M. Tatsumisago, *Journal of Power Sources*, 2016, **309**, 27-32.

105.   M. Nagao, A. Hayashi and M. Tatsumisago, *Bulk-Type Lithium Metal Secondary Battery with Indium Thin Layer at Interface between Li Electrode and Li2S-P2S5 Solid Electrolyte*, 2012.

106.   Z. Zhang, S. Chen, J. Yang, J. Wang, L. Yao, X. Yao, P. Cui and X. Xu, *ACS Applied Materials & Interfaces*, 2018, **10**, 2556-2565.

107.   G. Sahu, Z. Lin, J. Li, Z. Liu, N. Dudney and C. Liang, *Energy & Environmental Science*, 2014, **7**, 1053-1058.

108.   C. Wang, Y. Zhao, Q. Sun, X. Li, Y. Liu, J. Liang, X. Li, X. Lin, R. Li, K. R. Adair, L. Zhang, R. Yang, S. Lu and X. Sun, *Nano Energy*, 2018, **53**, 168-174.

109.   Y. Gao, D. Wang, Y. C. Li, Z. Yu, T. E. Mallouk and D. Wang, *Angewandte Chemie (International ed. in English)*, 2018, **57**, 13608-13612.

110.   M. A. Philip, P. T. Sullivan, R. Zhang, G. A. Wooley, S. A. Kohn and A. A. Gewirth, *ACS Applied Materials & Interfaces*, 2019, **11**, 2014-2021.

111.   Y. Sun, W. Yan, L. An, B. Wu, K. Zhong and R. Yang, *Solid State Ionics*, 2017, **301**, 59-63.

112.   Y. Sun, K. Suzuki, K. Hara, S. Hori, T.-a. Yano, M. Hara, M. Hirayama and R. Kanno, *Journal of Power Sources*, 2016, **324**, 798-803.

113.   R.-c. Xu, X.-h. Xia, X.-l. Wang, Y. Xia and J.-p. Tu, *Journal of Materials Chemistry A*, 2017, **5**, 2829-2834.

114.   G. Liu, D. Xie, X. Wang, X. Yao, S. Chen, R. Xiao, H. Li and X. Xu, *Energy Storage Materials*, 2019, **17**, 266-274.

115.   Z. Zhang, L. Zhang, X. Yan, H. Wang, Y. Liu, C. Yu, X. Cao, L. van Eijck and B. Wen, *Journal of Power Sources*, 2019, **410-411**, 162-170.

116.   P. Lu, F. Ding, Z. Xu, J. Liu, X. Liu and Q. Xu, *Study on (100-x)(70Li 2 S-30P 2 S 5)-xLi 2 ZrO 3 glass-ceramic electrolyte for all-solid-state lithium-ion batteries*, 2017.

117.   K. Minami, A. Hayashi and M. Tatsumisago, *Electrical and electrochemical properties of the 70Li2S·(30 − x)P2S5·xP2O5 glass-ceramic electrolytes*, 2008.

118.   K. Minami, F. Mizuno, A. Hayashi and M. Tatsumisago, *Journal of Non-Crystalline Solids*, 2008, **354**, 370-373.

119.   T. Ohtomo, F. Mizuno, A. Hayashi, K. Tadanaga and M. Tatsumisago, *Journal of Power Sources*, 2005, **146**, 715-718.

120.   Y. Tao, S. Chen, D. Liu, G. Peng, X. Yao and X. Xu, *Journal of The Electrochemical Society*, 2016, **163**, A96-A101.

121.   D. Xie, S. Chen, Z. Zhang, J. Ren, L. Yao, L. Wu, X. Yao and X. Xu, *Journal of Power Sources*, 2018, **389**, 140-147.

122.   Q. Ge, L. Zhou, Y.-m. Lian, X. Zhang, R. Chen and W. Yang, *Electrochemistry Communications*, 2018, **97**, 100-104.

123.   H.-D. Lim, H.-K. Lim, X. Xing, B.-S. Lee, H. Liu, C. Coaty, H. Kim and P. Liu, *Advanced Materials Interfaces*, 2018, **5**, 1701328.

124. X. Xu, G. Hou, X. Nie, Q. Ai, Y. Liu, J. Feng, L. Zhang, P. Si, S. Guo and L. Ci, *Journal of Power Sources*, 2018, **400**, 212-217.
125. J. Zhang, C. Zheng, J. Lou, Y. Xia, C. Liang, H. Huang, Y. Gan, X. Tao and W. Zhang, *Journal of Power Sources*, 2019, **412**, 78-85.
126. K. Fu, Y. Gong, B. Liu, Y. Zhu, S. Xu, Y. Yao, W. Luo, C. Wang, S. D. Lacey, J. Dai, Y. Chen, Y. Mo, E. Wachsman and L. Hu, *Science Advances*, 2017, **3**, e1601659.
127. C. Wang, Q. Sun, Y. Liu, Y. Zhao, X. Li, X. Lin, M. N. Banis, M. Li, W. Li, K. R. Adair, D. Wang, J. Liang, R. Li, L. Zhang, R. Yang, S. Lu and X. Sun, *Nano Energy*, 2018, **48**, 35-43.
128. M. Wang and J. Sakamoto, *Journal of Power Sources*, 2018, **377**, 7-11.
129. W. Xia, B. Xu, H. Duan, X. Tang, Y. Guo, H. Kang, H. Li and H. Liu, *Journal of the American Ceramic Society*, 2017, **100**, 2832-2839.
130. L. Cheng, E. J. Crumlin, W. Chen, R. Qiao, H. Hou, S. Franz Lux, V. Zorba, R. Russo, R. Kostecki, Z. Liu, K. Persson, W. Yang, J. Cabana, T. Richardson, G. Chen and M. Doeff, *Physical Chemistry Chemical Physics*, 2014, **16**, 18294-18300.
131. Y. Li, X. Chen, A. Dolocan, Z. Cui, S. Xin, L. Xue, H. Xu, K. Park and J. B. Goodenough, *Journal of the American Chemical Society*, 2018, **140**, 6448-6455.
132. L. Cheng, W. Chen, M. Kunz, K. Persson, N. Tamura, G. Chen and M. Doeff, *ACS Applied Materials & Interfaces*, 2015, **7**, 2073-2081.
133. Y. Lu, X. Huang, Y. Ruan, Q. Wang, R. Kun, J. Yang and Z. Wen, *Journal of Materials Chemistry A*, 2018, **6**, 18853-18858.
134. W. Luo, Y. Gong, Y. Zhu, K. K. Fu, J. Dai, S. D. Lacey, C. Wang, B. Liu, X. Han, Y. Mo, E. D. Wachsman and L. Hu, *Journal of the American Chemical Society*, 2016, **138**, 12258-12262.
135. W. Luo, Y. Gong, Y. Zhu, Y. Li, Y. Yao, Y. Zhang, K. Fu, G. Pastel, C.-F. Lin, Y. Mo, E. D. Wachsman and L. Hu, *Advanced Materials*, 2017, **29**, 1606042.
136. X. Han, Y. Gong, K. Fu, X. He, G. T. Hitz, J. Dai, A. Pearse, B. Liu, H. Wang, G. Rubloff, Y. Mo, V. Thangadurai, E. D. Wachsman and L. Hu, *Nature Materials*, 2016, **16**, 572.
137. K. Fu, Y. Gong, Z. Fu, H. Xie, Y. Yao, B. Liu, M. Carter, E. Wachsman and L. Hu, *Angewandte Chemie International Edition*, 2017, **56**, 14942-14947.
138. C. Wang, Y. Gong, B. Liu, K. Fu, Y. Yao, E. Hitz, Y. Li, J. Dai, S. Xu, W. Luo, E. D. Wachsman and L. Hu, *Nano Letters*, 2017, **17**, 565-571.
139. Y. Shao, H. Wang, Z. Gong, D. Wang, B. Zheng, J. Zhu, Y. Lu, Y.-S. Hu, X. Guo, H. Li, X. Huang, Y. Yang, C.-W. Nan and L. Chen, *ACS Energy Letters*, 2018, **3**, 1212-1218.
140. H. Xu, Y. Li, A. Zhou, N. Wu, S. Xin, Z. Li and J. B. Goodenough, *Nano Letters*, 2018, **18**, 7414-7418.
141. W. Zhou, Y. Zhu, N. Grundish, X. Sen, S. Wang, Y. You, N. Wu, J. Gao, Z. Cui, Y. Li and J. B. Goodenough, *Nano Energy*, 2018, **53**, 926-931.
142. B. Liu, Y. Gong, K. Fu, X. Han, Y. Yao, G. Pastel, C. Yang, H. Xie, E. D. Wachsman and L. Hu, *ACS Applied Materials & Interfaces*, 2017, **9**, 18809-18815.
143. B. Xu, W. Li, H. Duan, H. Wang, Y. Guo, H. Li and H. Liu, *Journal of Power Sources*, 2017, **354**, 68-73.
144. Z. Wang, Z. Wang, L. Yang, H. Wang, Y. Song, L. Han, K. Yang, J. Hu, H. Chen and F. Pan, *Nano Energy*, 2018, **49**, 580-587.
145. Y. Tian, F. Ding, H. Zhong, C. Liu, Y.-B. He, J. Liu, X. Liu and Q. Xu, *Li 6.75 La 3 Zr 1.75 Ta 0.25 O 12 @Amorphous Li 3 OCl Composite Electrolyte for Solid State Lithium-metal Batteries*, 2018.
146. S.-S. Chi, Y. Liu, N. Zhao, X. Guo, C.-W. Nan and L.-Z. Fan, *Energy Storage Materials*, 2019, **17**, 309-316.
147. C. Yang, L. Zhang, B. Liu, S. Xu, T. Hamann, D. McOwen, J. Dai, W. Luo, Y. Gong, E. D. Wachsman and L. Hu, *Proceedings of the National Academy of Sciences*, 2018, **115**, 3770-3775.

148.   Y. Liu, D. Lin, Y. Jin, K. Liu, X. Tao, Q. Zhang, X. Zhang and Y. Cui, *Science Advances*, 2017, **3**, eaao0713.
149.   K. Fu, Y. Gong, G. T. Hitz, D. W. McOwen, Y. Li, S. Xu, Y. Wen, L. Zhang, C. Wang, G. Pastel, J. Dai, B. Liu, H. Xie, Y. Yao, E. D. Wachsman and L. Hu, *Energy & Environmental Science*, 2017, **10**, 1568-1575.
150.   J. Bae, Y. Li, J. Zhang, X. Zhou, F. Zhao, Y. Shi, J. B. Goodenough and G. Yu, *Angewandte Chemie International Edition*, 2018, **57**, 2096-2100.
151.   D. Li, L. Chen, T. Wang and L.-Z. Fan, *ACS Applied Materials & Interfaces*, 2018, **10**, 7069-7078.
152.   J. Zheng, M. Tang and Y. Y. Hu, *Angewandte Chemie International Edition*, 2016, **55**, 12538-12542.
153.   X. Zhang, T. Liu, S. Zhang, X. Huang, B. Xu, Y. Lin, B. Xu, L. Li, C.-W. Nan and Y. Shen, *Journal of the American Chemical Society*, 2017, **139**, 13779-13785.
154.   K. K. Fu, Y. Gong, J. Dai, A. Gong, X. Han, Y. Yao, C. Wang, Y. Wang, Y. Chen and C. Yan, *Proceedings of the National Academy of Sciences*, 2016, **113**, 7094-7099.
155.   Y. Zhao, C. Wu, G. Peng, X. Chen, X. Yao, Y. Bai, F. Wu, S. Chen and X. Xu, *Journal of Power Sources*, 2016, **301**, 47-53.
156.   J. Ju, Y. Wang, B. Chen, J. Ma, S. Dong, J. Chai, H. Qu, L. Cui, X. Wu and G. Cui, *ACS applied materials & interfaces*, 2018, **10**, 13588-13597.
157.   C.-P. Yang, Y.-X. Yin, S.-F. Zhang, N.-W. Li and Y.-G. Guo, *Nature Communications*, 2015, **6**, 8058.
158.   S. Liu, A. Wang, Q. Li, J. Wu, K. Chiou, J. Huang and J. Luo, *Joule*, 2018, **2**, 184-193.
159.   D. Lin, Y. Liu, Z. Liang, H.-W. Lee, J. Sun, H. Wang, K. Yan, J. Xie and Y. Cui, *Nature Nanotechnology*, 2016, **11**, 626.
160.   S.-S. Chi, Y. Liu, W.-L. Song, L.-Z. Fan and Q. Zhang, *Advanced Functional Materials*, 2017, **27**, 1700348.
161.   L. Porz, T. Swamy, B. W. Sheldon, D. Rettenwander, T. Frömling, H. L. Thaman, S. Berendts, R. Uecker, W. C. Carter and Y. M. Chiang, *Advanced Energy Materials*, 2017, **7**, 1701003.
162.   F. Han, A. S. Westover, J. Yue, X. Fan, F. Wang, M. Chi, D. N. Leonard, N. J. Dudney, H. Wang and C. Wang, *Nature Energy*, 2019, 1.

Table of Content
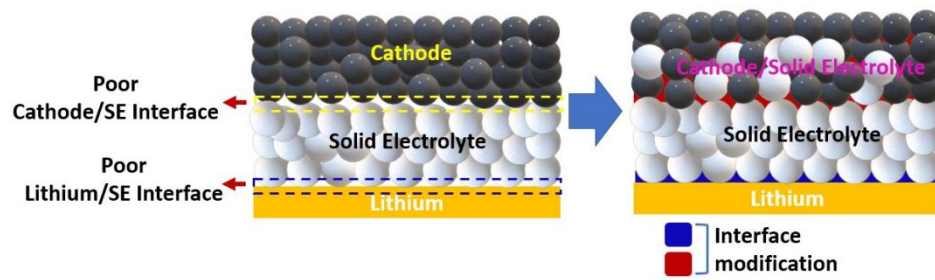
This review focuses on recent advances in interface engineering of solid-state batteries based on inorganic oxide and sulfide solid electrolytes.